# Localization dynamics of endogenous fluorescently labeled RAF1 in EGF-stimulated cells

Sachin V. Surve[a], Paul J. Myers[b], Samantha A. Clayton[c], Simon C. Watkins[a], Matthew J. Lazzara[b,c], and Alexander Sorkin[a,*]

[a]Department of Cell Biology, University of Pittsburgh School of Medicine, Pittsburgh, PA 15261; [b]Department of Chemical Engineering and [c]Department of Biomedical Engineering, University of Virginia, Charlottesville, VA 22904

**ABSTRACT** **Activation of the epidermal growth factor (EGF) receptor (EGFR) at the cell surface initiates signaling through the RAS-RAF-MAPK/ERK1/2 pathway and receptor endocytosis. Whether this signaling continues from endosomes remains unclear, because RAS is predominantly located on the plasma membrane, and the localization of endogenous RAF kinases, downstream effectors of RAS, is not defined. To examine RAF localization, we labeled endogenous RAF1 with mVenus using gene editing. From 10 to 15% of RAF1-mVenus (<2000 molecules/cell), which was initially entirely cytosolic, transiently translocated to the plasma membrane after EGF stimulation. Following an early burst of translocation, the membrane-associated RAF1-mVenus was undetectable by microscopy or subcellular fractionation, and this pool was estimated to be <200 molecules per cell. In contrast, persistent EGF-dependent translocation of RAF1-mVenus to the plasma membrane was driven by the RAF inhibitor sorafenib, which increases the affinity of Ras-GTP:RAF1 interactions. RAF1-mVenus was not found in EGFR-containing endosomes under any conditions. Computational modeling of RAF1 dynamics revealed that RAF1 membrane abundance is controlled most prominently by association and dissociation rates from RAS-GTP and by RAS-GTP concentration. The model further suggested that the relatively protracted activation of the RAF-MEK1/2-ERK1/2 module, in comparison with RAF1 membrane localization, may involve multiple rounds of cytosolic RAF1 rebinding to active RAS at the membrane.**

**Monitoring Editor**
Carl-Henrik Heldin
Ludwig Institute for Cancer Research

Received: Aug 16, 2018
Revised: Dec 14, 2018
Accepted: Dec 18, 2018

## INTRODUCTION

The RAS-MAPK/ERK1/2 (mitogen-activated protein kinase/extracellular stimuli–regulated kinase 1/2) signaling pathway is involved in the regulation of all major cell behaviors, including survival, growth, proliferation, differentiation, and motility (Cargnello and Roux, 2011). This signaling axis is one of the key tumorigenic drivers, and in recent years it has become the major target for cancer therapy (Samatar and Poulikakos, 2014). RAS is activated by growth factors, hormones, adhesion, and other receptors. In one of the best-studied systems, epidermal growth factor (EGF) receptor (EGFR) activates RAS by recruiting a complex of an adaptor protein Grb2 and RAS GDP–GTP exchange factor, son of sevenless (SOS), to the plasma membrane, thus activating membrane-associated RAS. GTP-loaded RAS, in turn, recruits RAF serine–threonine kinases (MAPKKKs) to the membrane, which leads to activation of the RAF kinase. Activated RAF kinase is capable of binding, phosphorylating, and activating MEK1 and 2 (MAPKKs). Sequentially, MEK1/2 kinases phosphorylate catalytic threonine and tyrosine residues in ERK1/2, leading to their activation.

The main steps of this pathway are understood at the molecular and biochemical levels, and various models have been proposed to describe how the amplitude and kinetics of ERK1/2 activation triggered by EGFR or other receptors are regulated. One of the major regulators of the dynamics of EGFR signaling to ERK1/2 is thought

This article was published online ahead of print in MBoC in Press (http://www.molbiolcell.org/cgi/doi/10.1091/mbc.E18-08-0512) on December 26, 2018.

*Address correspondence to: Alexander Sorkin (sorkin@pitt.edu).

Abbreviations used: CFP, YFP, and RFP, cyan, yellow, and red fluorescent proteins, respectively; EGF, epidermal growth factor; EGFR, EGF receptor; MAPK/ERK1/2, mitogen-activated protein kinase/extracellular stimuli–regulated kinase 1/2; PLSR, partial least-squares regression; SOS, son of sevenless; TIRF, total internal reflection fluorescence.

to be endocytic trafficking. Ligand binding results in rapid internalization of EGFR and accumulation of the bulk of active EGFR in endosomes, especially in cells with low or moderate levels of EGFRs (<50,000/cell). Whether signaling along the RAS-ERK1/2 axis continues in endosomes and whether such extension of signaling in time is responsible for the sustained activity of ERK1/2 are under debate (reviewed in Sorkin and Von Zastrow, 2002). When general inhibitors of endocytosis are used, contrasting effects on EGF-induced ERK1/2 activation have been reported (Vieira *et al.*, 1996; Johannessen *et al.*, 2000; Teis *et al.*, 2002; Sousa *et al.*, 2012). On the other hand, localization and trafficking of the receptor-downstream components of the pathway in stimulated cells are not well defined, and evidence for the endosome signaling hypothesis is mainly based on studies with overexpressed proteins or disrupted cells (by subcellular fractionation). We have previously examined the localization of fluorescently labeled Grb2 expressed at the physiological level and found that EGFR–Grb2 complexes are maintained and accumulate in endosomes in HeLa cells during at least the first hour of cell stimulation by EGFR ligands (Fortian and Sorkin, 2014). Unexpectedly, endogenous HRAS was not present in endosomes containing EGFR–Grb2 complexes in the same cells (Pinilla-Macua *et al.*, 2016). Moreover, there was very little, if any, targeting of overexpressed KRAS and NRAS to EGFR-containing endosomes in HeLa cells. Paradoxically, EGF-induced MEK1/2 and ERK1/2 activities were found still to be dependent on the activity of the EGFR kinase even after physical separation of Ras from EGFR in the cell (Pinilla-Macua *et al.*, 2016). It is possible that a small pool of EGFRs remaining at the cell surface is sufficient to sustain RAS-dependent activation of RAF and subsequent activation of MEK1/2 and ERK1/2. Alternatively, signaling from endosomal EGFRs to the plasma membrane RAS is mediated by some diffusible species such as active SHP2 (Furcht *et al.*, 2015). Finally, signaling from endosomal EGFR to RAF-MEK-ERK may be mediated in an RAS-independent manner by an unknown mechanism.

The RAS-dependent activation of RAF is perhaps the most complex and least understood step in the ERK activation pathway, because it is regulated by RAF dimerization and multiple phosphorylation/dephosphorylation events, as well as interactions with and activities of several additional proteins (Matallanas *et al.*, 2011; Lavoie and Therrien, 2015). All three RAF kinases, RAF1, ARAF, and especially BRAF, are expressed at low levels, as compared with RAS (upstream) and MAP kinases (downstream), in most cell types, and therefore, RAF activation likely represents a "bottleneck" in the pathway (Fujioka *et al.*, 2006; Shi *et al.*, 2016). BRAF is the most evolutionarily conserved, and it was proposed that heterodimers of BRAF and RAF1 are predominant species that appear to be most important for signaling to ERK1/2 in HeLa cells (Matallanas *et al.*, 2011; Freeman *et al.*, 2013; Lavoie and Therrien, 2015).

The kinetics of RAF translocation to the membrane, the relationship of the kinetics of its membrane association with activation/deactivation, and the subcellular locations of RAF activation by the EGFR–RAS signaling axis remain sparsely studied and are not fully characterized. While signal-induced translocation of overexpressed fluorescently tagged or endogenous RAF from the cytosol to the plasma membrane and endosomes was demonstrated using, respectively, microscopy imaging (e.g., Rizzo *et al.*, 2000; Anderson *et al.*, 2011) or subcellular fractionation (Pol *et al.*, 1998; Wu *et al.*, 2001), other studies did not detect translocation of full-length RAF to the plasma membrane or endosomes in EGF-stimulated cells (e.g., Bondeva *et al.*, 2002; McKay *et al.*, 2011). Localization of endogenous RAF in endosomes containing insulin receptor was shown by immunofluorescence in Rat-1 cells (Rizzo *et al.*, 2000).

Because of an extremely low level of BRAF expression (Kulak *et al.*, 2014), live-cell optical imaging studies of endogenous BRAF are not feasible. Hence, to examine the dynamics of endogenous RAF proteins in living cells stimulated with EGF, we used the CRISPR/Cas9 gene-editing method to tag RAF1 with the mVenus fluorescent protein in HeLa cells. RAF1 is the physiologically important isoform as its mouse knockout results in defects in organ development and embryonic lethality (Wojnowskia *et al.*, 1998; Mikula *et al.*, 2001; Leicht *et al.*, 2007). Live-cell microscopy imaging, subcellular fractionation, and computational modeling were used to describe the dynamics of subcellular localization of RAF1-mVenus in cells stimulated with EGF quantitatively and determine kinetic parameters that control this dynamics.

## RESULTS

### Generation and characterization of endogenous mVenus–tagged RAF1

To study the localization of endogenous RAF1, mVenus fluorescent protein (a pH-insensitive mutant of yellow fluorescent protein, YFP) was inserted at the carboxyl terminus of the RAF1 protein using the CRISPR/Cas9 genome-editing method in HeLa cells (Figure 1A). These HeLa cells have been used previously in our studies of the localization of other components of the EGFR–ERK1/2 signaling pathway, such as Grb2, RAS, and MEK2 (Galperin and Sorkin, 2008; Fortian and Sorkin, 2014; Pinilla-Macua *et al.*, 2016). They express a moderate level of EGFR at the cell surface (~40,000/cell), which is within the range of EGFR expression by normal epithelial cells. To engineer RAF1-mVenus, guide RNAs (gRNAs), Cas9, and the donor vector containing the mVenus sequence were transfected into cells, and single-cell clones were selected that expressed RAF1-mVenus. Two rounds of transfection and clone selection were carried out to obtain a cell clone (#23) in which mVenus was inserted into both alleles of the *RAF1* gene. The insertion of mVenus in this clone (further referred to as HeLa/RAF1-mVenus cells) was demonstrated by PCR of the genomic DNA (Figure 1B) and Western blotting (Figure 1C).

To confirm the functionality of RAF1-mVenus, the kinetics of EGF-induced RAF1 phosphorylation at one of its activation sites (Ser338) and of phosphorylation of the RAF substrate MEK1/2 were compared in parental HeLa and HeLa/RAF1-mVenus cells. As shown in Figure 1D, the time course of RAF1-mVenus phosphorylation was similar to that of the wild-type RAF1 in parental cells. The time courses of MEK1/2 and ERK1/2 phosphorylation were also similar in parental and genome-edited HeLa cells. These data validate the HeLa/RAF1-mVenus cells as an appropriate model for studying endogenous RAF1 localization and its dynamics.

### RAF1-mVenus is predominantly cytoplasmic and transiently translocates to the plasma membrane, but not to endosomes, upon cell stimulation with EGF

To examine subcellular localization of RAF1-mVenus, live-cell imaging of HeLa/RAF1-mVenus cells was performed at 37°C using a spinning-disk confocal microscope. RAF1-mVenus was diffusely distributed within the cytoplasm (Figure 2A). The intensity of mVenus fluorescence was rather low; thus, imaging required maximum laser power and long image acquisition times. Such weak fluorescence of RAF1-mVenus is consistent with the low copy number of the RAF1 protein in HeLa and other cells determined using biochemical methods (Nagaraj *et al.*, 2011; Shi *et al.*, 2016). In addition to the diffuse cytosolic fluorescence, vesicular-like compartments located mostly in the perinuclear area of the cells were detected through the 515 nm channel (Figure 2A).

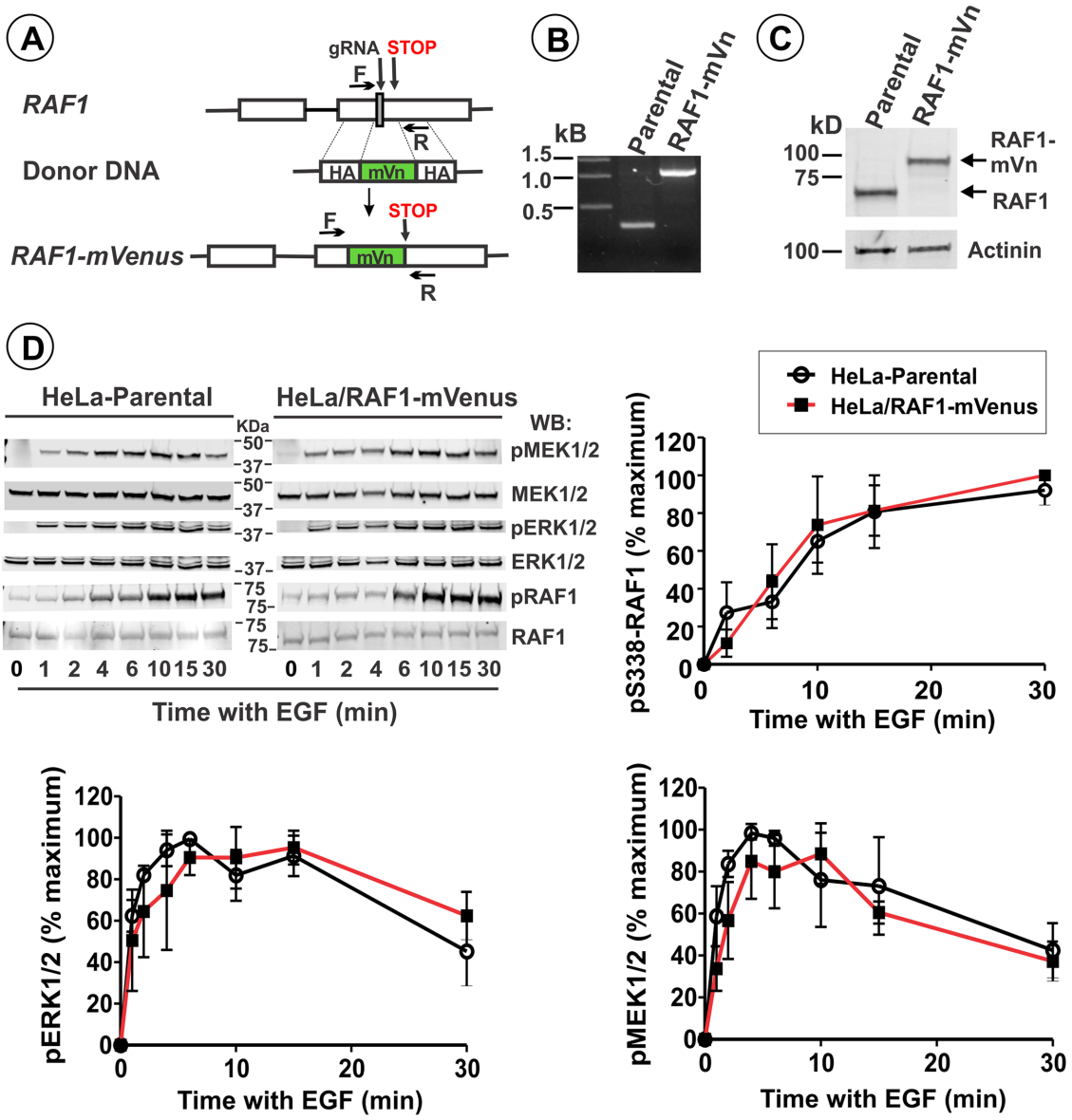


FIGURE 1: Generation and characterization of HeLa cells expressing endogenous RAF1-mVenus. (A) Schematics of the insertion of the mVenus sequence into the endogenous locus in the *RAF1* gene. See details in *Materials and Methods*. gRNA, guide RNA. F, forward primer. R, reverse primer. (B) F and R primers were used to confirm the insertion of the mVenus sequence at the correct locus of the RAF1 gene using the PCR. Expected size of PCR product was 320 and 1066 base pairs in wild-type and RAF1-mVenus genomic DNAs, respectively. (C) Lysates of parental HeLa and HeLa/RAF1-mVenus cells were probed by Western blotting with RAF1 and α-actinin antibodies (loading control). mVn, mVenus. (D) Parental HeLa and HeLa/RAF1-mVenus cells were serum starved and treated with 4 ng/ml EGF for 0–30 min at 37°C. Cell lysates were electrophoresed and probed by Western blotting with antibodies to pSer338 of RAF1, RAF1, phosphoMEK1/2, MEK1/2, phosphoERK1/2, and ERK1/2. See full-size pRAF1 and RAF1 blots in Supplemental Figure S1. The values of the ratios of a phosphoprotein to the total amount of the same protein were normalized to the maximal value of the ratio in each time course and plotted against time. The data on the graph plots are mean values from three independent experiments (±SEM).

The predominantly cytosolic localization of RAF1-mVenus was mostly unchanged in cells stimulated with unlabeled EGF or EGF-rhodamine (EGF-Rh). RAF1-mVenus fluorescence was observed to concentrate in plasma membrane ruffles and protrusions, and at cell edges between 1 and 8 min after EGF-Rh (4 ng/ml) stimulation (Figure 2A). To directly prove plasma membrane translocation and estimate the membrane fraction of RAF1-mVenus, HeLa/RAF1-mVenus cells were stained with CellMask, which marks cellular membranes, and then treated with EGF-Rh at 37°C. There was no visible colocalization of CellMask and RAF1-mVenus in serum-starved cells (Figure 3A). Colocalization of CellMask and RAF1-mVenus was, however, evident in the plasma membrane protrusions and cell edges in cells treated with EGF-Rh for 1–8 min (Figure 3A; the 5-min time point is shown). Previous studies demonstrated the presence of endogenous mVenus-HRAS in similar plasma membrane structures in the same HeLa cells (Pinilla-Macua *et al.*, 2016). An apparent concentration of RAF1-mVenus fluorescence in protrusions and cell edges is likely due to overlapping membranes in these structures

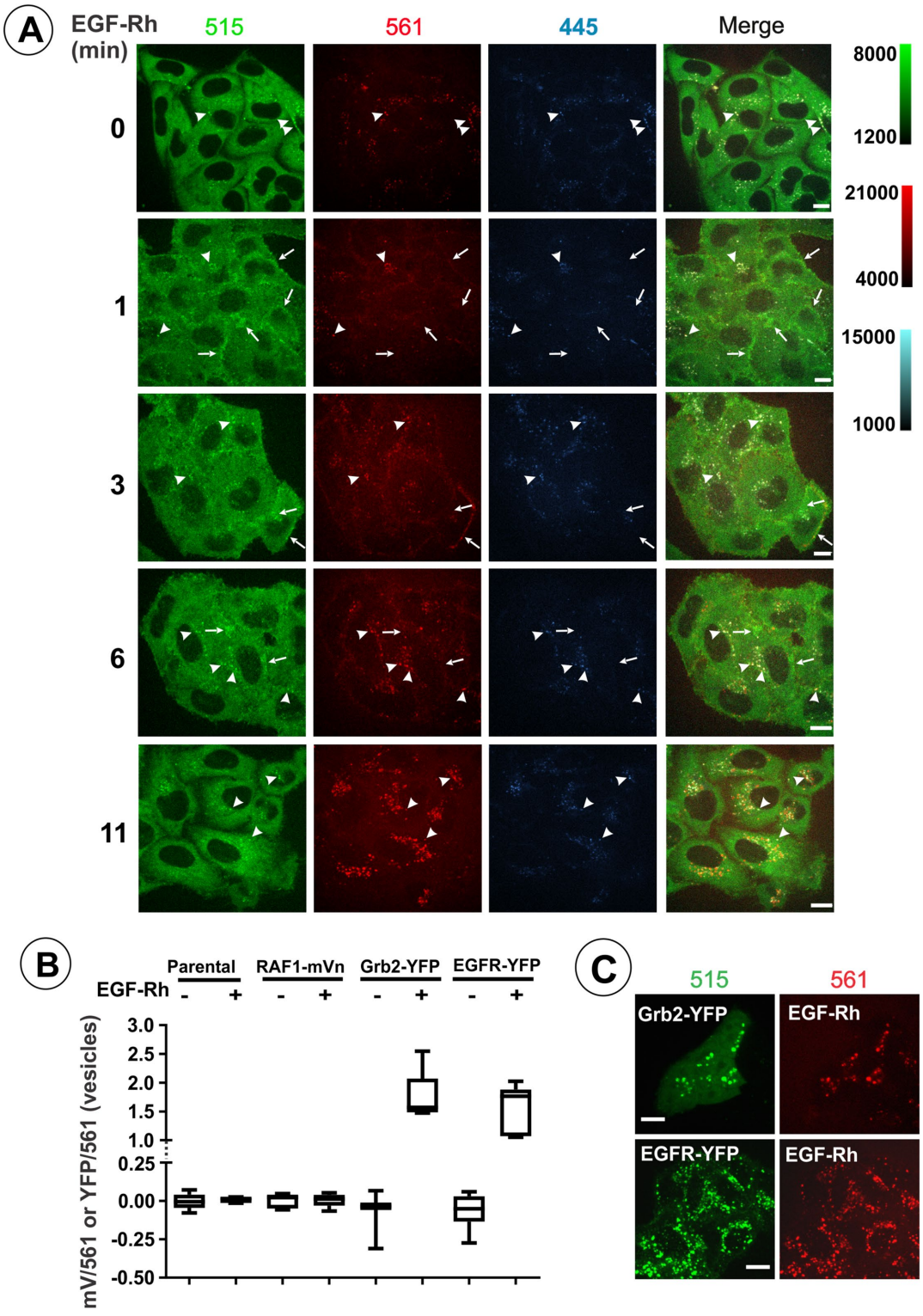


FIGURE 2: Localization of RAF1-mVenus in EGF-stimulated cells. (A) HeLa/RAF1-mVenus cells were serum starved and treated with 4 ng/ml EGF-Rh for 0–15 min at 37°C. Three-dimensional live-cell imaging was performed through 445 nm (cyan), 515 nm (green), and 561 nm (red) filter channels. Fluorescence intensity scales are identical for images at all time points (shown to the right of images). Individual confocal sections are shown. Arrows point out examples of the plasma membrane localization of RAF1-mVenus. Arrowheads point out examples of vesicular fluorescence. Scale bars, 10 μm. (B) Parental HeLa, Hela/RAF1-mVenus, HeLa/Grb2-YFP cells, and HeLa cells transiently expressing EGFR-YFP were treated with 4 ng/ml EGF-Rh for 10 min and imaged as described in A. Quantification of background fluorescence through 515-nm channel, specific fluorescence intensities through 515- and 561-nm channels, and their ratios (mV/561 and YFP/561) in vesicles were performed as described in *Materials and Methods*. (C) Examples of the images of HeLa/Grb2-YFP cells and HeLa cells expressing EGFR-YFP incubated with EGF-Rh used for calculations of the YFP/561 ratio in B. Scale bars, 10 μm.

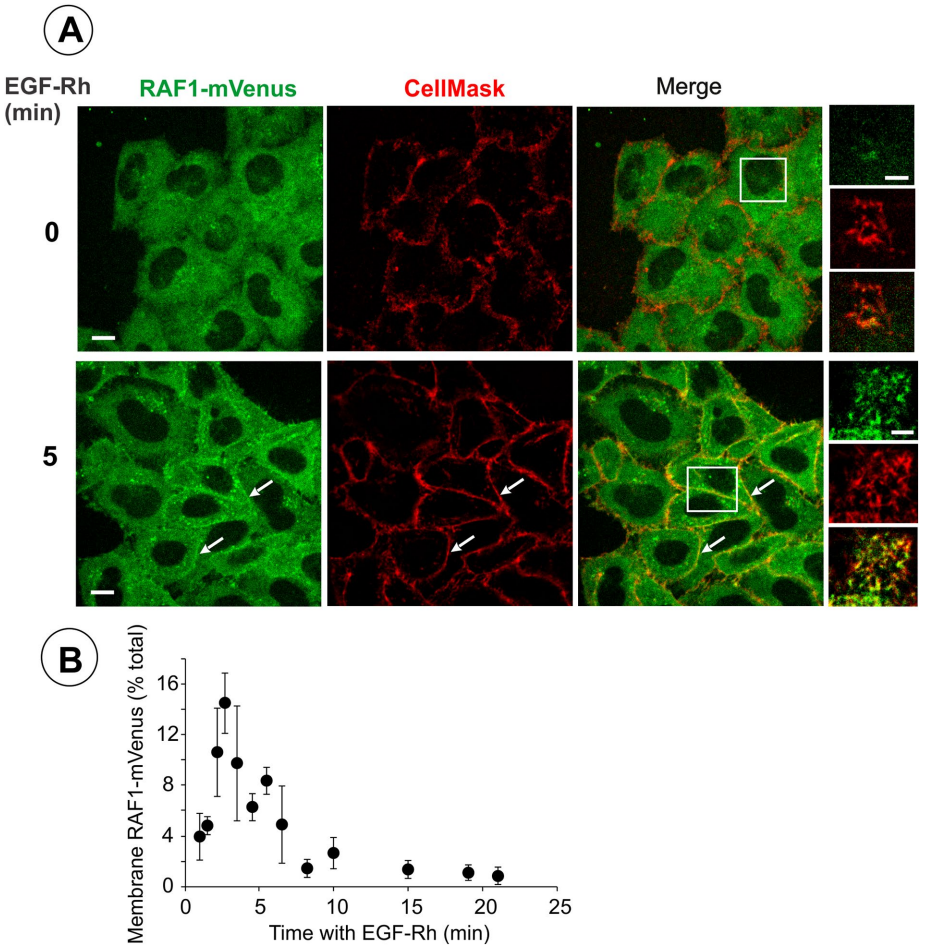


**FIGURE 3:** RAF1-mVenus membrane translocation in EGF-stimulated cells. (A) HeLa/RAF1-mVenus cells were serum starved, preincubated with CellMask to stain cellular membranes, washed, and then incubated with EGF-Rh (4 ng/ml) at 37°C. Live-cell three-dimensional imaging was performed through 515-nm (green, mVenus), 561-nm (rhodamine, not shown), and 640-nm (red, CellMask) channels. Individual confocal sections close to the bottom cell membrane from three-dimensional images of cells before and after 5-min incubation with EGF-Rh are shown. Arrows show examples of the plasma membrane localization of RAF1-mVenus. On the right, insets are the high-magnification images corresponding to the regions indicated by white rectangles and representing confocal sections through the tops of the cells depicting numerous membrane protrusions. (B) Quantification of the fraction of RAF1-mVenus colocalized with CellMask as a percentage of the total cellular RAF1-mVenus from three independent experiments exemplified in A was performed as described in *Materials and Methods*. In these quantifications, the mean value of the fraction measured in unstimulated cells was considered as background because the overlap of mVenus and CellMask fluorescence signals in unstimulated cells is due to insufficient resolution. This value (0.081 ± –0.008, SEM) was subtracted from all values of the membrane fractions of RAF1-mVenus measured in EGF-Rh–stimulated cells.

and regions, as evidenced by increased CellMask signals in the same structures and regions (Figure 3A). Quantification of RAF1-mVenus and CellMask colocalization revealed that up to 10–15% of total cellular RAF1-mVenus was transiently translocated to the plasma membrane upon EGFR activation (Figure 3B).

Images in Figures 2 and 3 show that some vesicles detected through the 515-nm channel also contained EGF-Rh, suggesting that RAF1-mVenus may be present on EGF-Rh–containing endosomes. However, an essentially similar pattern of vesicular fluorescence was observed in parental HeLa cells (Supplemental Figure S2). Moreover, vesicular compartments detected by excitation at 515 nm in parental or unstimulated gene-edited cells were also detected by imaging through 561- and 445-nm channels (Figure 2A), suggesting that the wide-spectrum fluorescence of these vesicles represents autofluorescence. We noticed that the ratios of apparent intensities of the vesicular fluorescence detected through 445-, 515-, and 561-nm channels were highly consistent within individual parental HeLa cells and between different cells if image acquisition parameters were kept constant. Therefore, to distinguish the autofluorescence signal from the specific mVenus fluorescence in HeLa/RAF1-mVenus cells, the ratio of the apparent fluorescence intensities detected through 515- and 445-nm channels ($I^{515}/I^{445}$) was measured using identical image acquisition parameters in multiple individual vesicles selected using segmentation based on the fluorescence through the 561-nm channel in parental HeLa cells and HeLa/RAF1-mVenus cells as described in *Materials and Methods*. The mean value of the $I^{515}/I^{445}$ ratio in parental cells ($k_{auto}$ = 2.59 ± 0.33 in experiments presented in Figure 2A; see *Materials and Methods*) was used to measure the autofluorescence and mVenus-specific components of the yellow (the 515-nm channel) fluorescence in the vesicles of HeLa/RAF1-mVenus cells. The ratio of the specific mVenus fluorescence to the red (561-nm channel) fluorescence (mV/561) was then calculated. These calculations showed that the fluorescence of endosomes containing EGF-Rh measured through the 515-nm channel in HeLa/RAF1-mVenus cells was solely due to the autofluorescence component (mV/561 ratios were effectively zero; see Figure 2B), indicating that these endosomes did not contain mVenus. In contrast, similar measurements in endosomes of HeLa cells expressing physiological levels of Grb2-YFP (Huang and Sorkin, 2005; Fortian and Sorkin, 2014) that were treated with EGF-Rh yielded high YFP/561 ratio values (Figure 2, B and C). Likewise, values of the YFP/561 ratio measured in EGF-Rh–containing endosomes of HeLa cells overexpressing EGFR–YFP were significantly higher than mV/561 values measured in HeLa/RAF1-mVenus cells (Figure 2B). These results demonstrate that specific accumulation of YFP- or mVenus-tagged proteins in EGF-Rh–containing endosomes can be detected faithfully after correction for autofluorescence using this simplified spectrum-unmixing method.

To estimate the minimum sensitivity threshold for detecting mVenus or YFP in endosomes, two approaches were used. First, fluorescence intensities of individual endosomes in EGF-Rh–treated cells expressing low levels of EGFR–YFP were measured as described in Figure 2B and compared with the intensities of endosomes in nontransfected cells. As shown in Supplemental Figure S3, specific endosomal YFP signals of ≥1000 arbitrary units of linear fluorescence intensity (a.u.l.f.i.) per image voxel were detected with high statistical

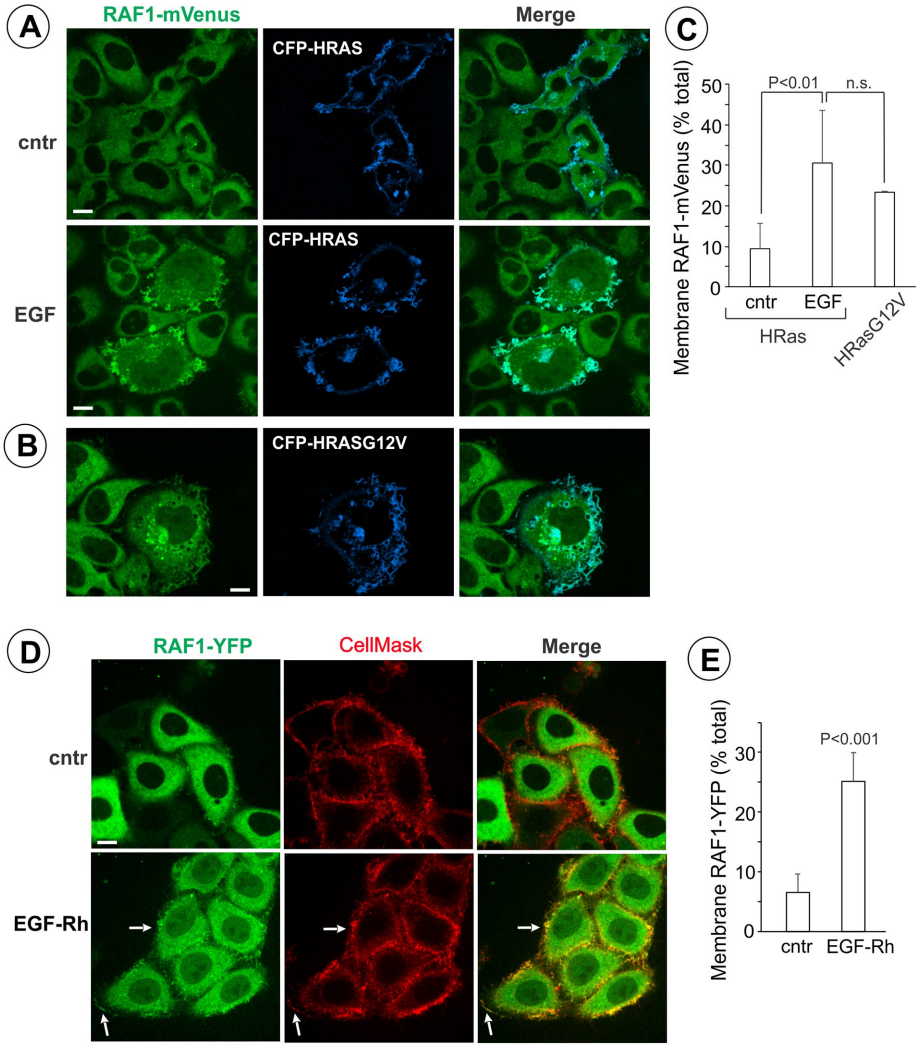


FIGURE 4: Effects of HRAS and RAF1 overexpression on RAF1 localization. (A) CFP-HRas was transiently expressed in HeLa/RAF1-mVenus cells. The cells were untreated (cntr) or incubated with 4 ng/ml EGF-Rh for 5 min at 37°C. Images were acquired from living cells through 445-nm (cyan, CFP), 515-nm (green, mVenus), and 561-nm (rhodamine, not shown) channels. Scale bar, 10 μm. (B) CFP-HRASG12V was transiently expressed in HeLa/RAF1-mVenus cells. Images were acquired from living cells through 445- nm (cyan, CFP) and 515-nm (green, mVenus) channels. Scale bar, 10 μm. (C) Quantification of the fraction of the total cellular RAF1-mVenus colocalized with CFP-HRAS or CFP-HRASG12V from experiments exemplified in A and B was performed as described in *Materials and Methods*. Bar graph represents mean values (±SD). n.s., difference is not significant. (D) RAF1-YFP was transiently expressed in parental HeLa cells. The cells were stained with CellMask and incubated or not (cntr) with EGF-Rh for 3.5 min at 37°C. Images were acquired from living cells through 515-nm (green, YFP) and 640-nm (red, CellMask) filter channels. Arrows point out on the examples of the plasma membrane localization of RAF1-YFP. Scale bars, 10 μm. (E) Quantification of the fraction of RAF1-YFP colocalized with CellMask of the total cellular RAF1-mVenus from experiments exemplified in D (incubation with EGF-Rh for 2–7 min) was performed as described in *Materials and Methods*. Bar graph represents mean values (±SD).

significance. In the second method, an apparent fluorescence intensity of individual plasma membrane structures containing RAF1-mVenus in EGF-stimulated cells was quantified after subtraction of the background of surrounding diffuse RAF1-mVenus fluorescence. The quantification yielded an average minimal intensity of those plasma membrane structures of ~2006 (SD 398) a.l.u.f.i/voxel (Supplemental Figure S3, A and C). Assuming that the apparent volume of the smallest endosome is 3 × 3 × 3 (27) voxels), calculations based on the apparent intensity of single mVenus molecules in these experiments (see *Materials and Methods*) suggest that the minimal detection threshold of mVenus fluorescence is 2–3 molecules per endosome.

### Plasma membrane translocation of RAF1 but not its endosomal localization is increased by overexpression of RAS or RAF1 and by the RAF kinase inhibitor

The data in Figures 2 and 3 show that RAF1-mVenus is mostly cytosolic upon cell stimulation with EGF-Rh, and that only a minor pool of RAF1-mVenus is transiently translocated to the plasma membrane. The inefficient detection of RAF1-mVenus on the plasma membrane and the lack of RAF1-mVenus in endosomes in EGF-stimulated cells could be due to relatively low levels of RAS GTP loading in EGF-stimulated cells, low abundance of endogenous RAF1, and/or highly transient kinetics of RAF1 binding to the membrane. We examined these possibilities in several sets of experiments.

First, we found that treatment of HeLa/RAF1-mVenus cells with a high concentration of EGF-Rh (100 ng/ml) did not increase the extent or duration of the plasma membrane translocation of RAF1-mVenus (Supplemental Figure S4). Further, to test whether a robust EGF-induced or constitutive activation of RAS elevates the recruitment of RAF1-mVenus to membranes, HeLa/RAF1-mVenus cells were transfected with CFP-tagged wild-type HRAS or constitutively active CFP-HRASG12V mutant. Live-cell imaging revealed increased and prolonged translocation of RAF1-mVenus to the plasma membrane upon cell stimulation with EGF-Rh as compared with that in cells not expressing CFP-HRAS (Figure 4, A and C). CFP-HRAS colocalization with RAF1-mVenus was especially evident in membrane protrusions (Figure 4A). In cells expressing CFP-HRASG12V, RAF1-mVenus was detected on the plasma membrane, which was most clearly observed in filopodia-like structures, although the bulk of RAF1-mVenus remained cytosolic (Figure 4, B and C). Small amounts of RAF1-mVenus were apparently associated with large endosomal vesicles that were forming due to CFP-HRASG12V–induced macropinocytosis (Figure 4B). Experiments with this RAS mutant confirmed that even under conditions of massive constitutive GTP loading of RAS, the pool of membrane-associated RAF1 is relatively small. Together, results in Figure 4 further imply that while the membrane pool of RAF1 depends on the concentration of GTP-RAS, there are additional factors that determine the upper limit of RAF1 membrane concentration.

Second, to test whether cellular concentration of RAF1 is a limiting factor, we ectopically overexpressed RAF1-YFP in parental HeLa

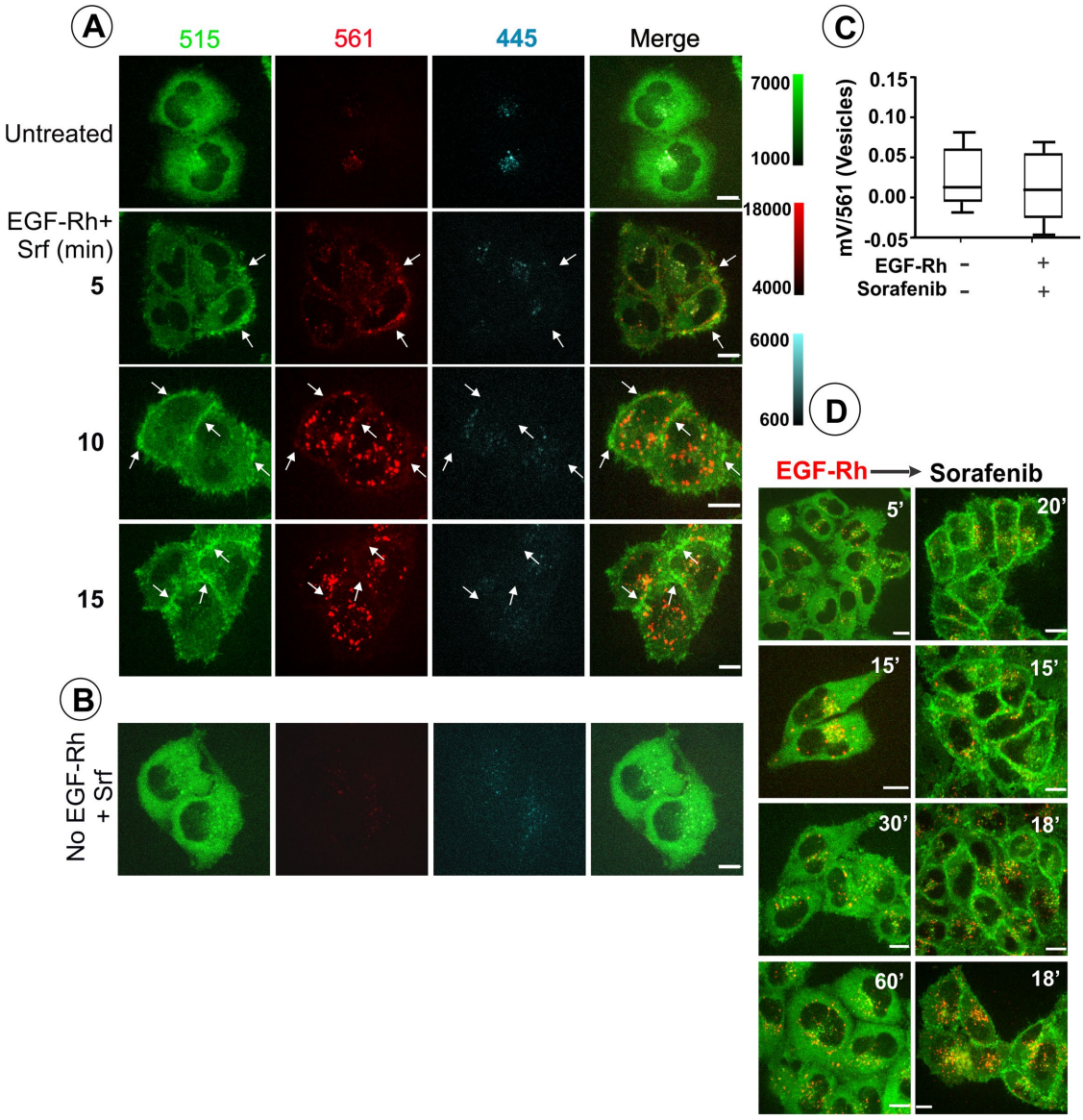


FIGURE 5: RAF1-mVenus is stabilized on the plasma membrane but not in endosomes of EGF-stimulated cells by sorafenib. (A) HeLa/RAF1-mVenus cells were serum starved and incubated with EGF-Rh (4 ng/ml) and sorafenib (10 μM) for 0 (Untreated)–15 min at 37°C. Live-cell imaging was performed as in Figure 2A. The arrows point out examples of the plasma membrane RAF1-mVenus. Scale bars, 10 μm. Dose–response experiments revealed that 10 μM sorafenib produced the greatest extent of EGF-dependent translocation of RAF1-mVenus to the plasma membrane. (B) HeLa/RAF1-mVenus cells were treated with sorafenib (10 μM) for 24 h at 37°C. Live cell imaging was performed as in A. Scale bar, 10 μm. (C) Quantification of the specific signal through the 515-nm channel and the ratio (*mV/561*) in vesicles of cells treated or not with EGF-Rh and sorafenib (representative images in A) was performed as described in *Materials and Methods* and Figure 2B. (D) HeLa/RAF1-mVenus cells were serum starved and incubated with EGF-Rh (4 ng/ml) for 5–60 min at 37°C and then treated with sorafenib (10 μM) for 5–30 min at 37°C. Live-cell imaging was performed as in Figure 2A. Representative images (single confocal sections) are shown. Scale bars, 10 μm.

cells. Transient EGF-induced translocation of overexpressed RAF1 to the plasma membrane, but not to endosomes, was observed more readily and frequently in cells expressing high levels of RAF1-YFP than in low expressors or HeLa/RAF1-mVenus cells (Figure 4D). These data suggest that there might be a threshold in the cellular concentration of RAF1 above which the membrane pool of RAF1 is stabilized at the membrane, although such stabilization does not extend the lifetime of RAF1 plasma membrane translocation.

Third, we took advantage of the previously published observation that inhibitors of the RAF kinase increase membrane priming of overexpressed RAF1 (Hatzivassiliou *et al.*, 2010; Poulikakos *et al.*, 2010; Anderson *et al.*, 2011). HeLa/RAF1-mVenus cells were treated with sorafenib (10 μM), a RAF kinase inhibitor, before and during cell stimulation with 4 ng/ml EGF-Rh. Live-cell imaging demonstrated that a significant amount of RAF1-mVenus was associated with the plasma membrane as early as 3–5 min after EGF stimulation, and this membrane localization reached a maximum after 15 min of EGF-Rh stimulation in the presence of sorafenib (Figure 5A). As in the absence of sorafenib (Figure 2), fluorescence through the 515-nm channel was detected in some EGF-Rh–containing endosomes in cells incubated with sorafenib (Figure 5A). However, correction for autofluorescence revealed that this signal is nonspecific

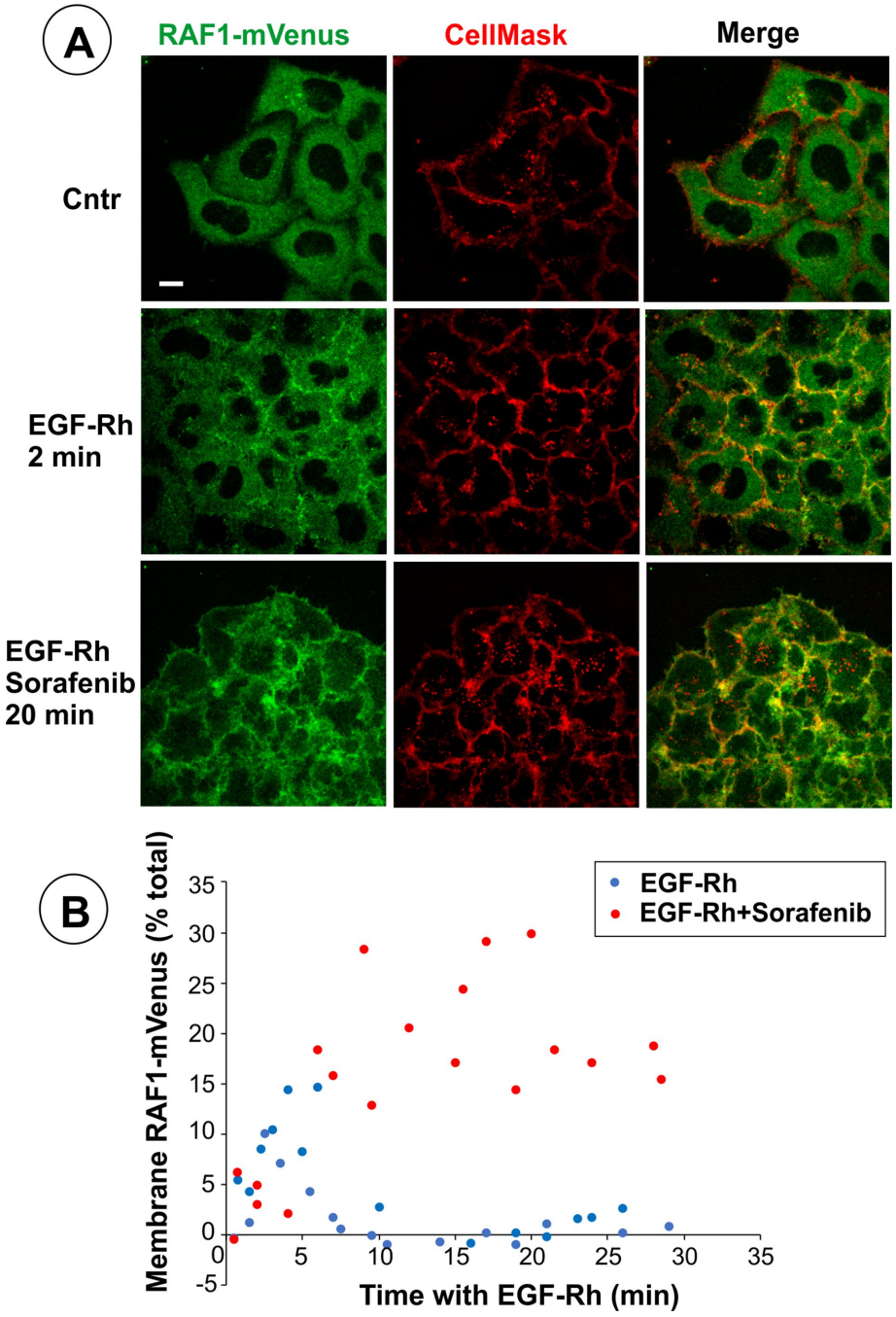


FIGURE 6: Time course of RAF1-mVenus membrane translocation upon EGF stimulation in the absence and presence of sorafenib. (A) HeLa/RAF1-mVenus cells were serum starved, preincubated with CellMask to stain cellular membranes, washed, and then incubated with EGF-Rh (4 ng/ml) alone or with sorafenib (10 μM) at 37°C. Live-cell three-dimensional imaging was performed through 515-nm (green, mVenus), 561-nm (not shown), and 640-nm (red, CellMask) channels. (B) Quantification of the fractions of RAF1-mVenus colocalized with CellMask of the total cellular RAF1-mVenus from images exemplified in A was performed as described in *Materials and Methods*. In these quantifications, the mean value of the fraction measured in unstimulated cells was considered as background because the overlap of mVenus and CellMask fluorescence signals in unstimulated cells is due to insufficient resolution. This value (0.026 ± 0.004, SEM) was subtracted from all values of the fraction of membrane-associated mVenus measured in stimulated cells.

and that RAF1-mVenus is not present in EGF-Rh–containing endosomes under conditions of enhanced plasma membrane recruitment of RAF1 (Figure 5C). Importantly, membrane translocation of endogenous RAF1-mVenus was not observed for up to 24 h of exposure of EGF-untreated cells to 10-μM sorafenib (Figure 5B, bottom), indicating that the EGFR activity (which is necessary for RAS activation) is essential for sorafenib-dependent membrane recruitment of RAF1. Surprisingly, RAF1-mVenus translocation to the plasma membrane was observed even when the cells were treated with sorafenib after 1-h EGF stimulation (Figure 5D). This observation demonstrates the presence of a pool of GTP-loaded RAS in the plasma membrane and predicts that RAF1-mVenus will continue to translocate to the plasma membrane during prolonged EGF stimulation without sorafenib, although under these conditions the translocation is highly transient and the membrane pool of RAF1 is too small to be faithfully detected by fluorescence microscopy.

To quantitatively compare the membrane translocation of RAF1-mVenus in cells treated with EGF-Rh alone or with EGFR-Rh plus sorafenib, the cells were stained with CellMask before stimulation, as described in experiments presented in Figure 3. Colocalization of CellMask and RAF1-mVenus was apparent in cells treated with EGF-Rh alone for 2–6 min, whereas in the presence of sorafenib, colocalization of RAF1-mVenus and CellMask was detected after a few minutes of EGF stimulation and then gradually increased and maintained for at least 30 min (Figure 6A). Quantification of colocalization showed that, whereas 10–15% of total cellular RAF1-mVenus was transiently translocated to the plasma membrane in EGF-Rh stimulated cells, up to 30% of cellular RAF1-mVenus was continuously associated with the plasma membrane in cells treated with EGF-Rh and sorafenib (Figure 6B). A significant number of CellMask-labeled membranes were internalized during incubation of cells at 37°C; however, no specific fluorescence of RAF1-mVenus was detected in endosomes labeled with CellMask (Figure 6A).

### Membrane translocation of RAF1-mVenus upon EGF stimulation detected by total internal reflection fluorescence imaging

Low cellular concentrations of RAF1-mVenus prevented time-lapse confocal imaging of RAF1-mVenus dynamics in single cells during EGF stimulation due to photobleaching. Therefore, we examined whether such time-lapse imaging could be performed using total internal reflection fluorescence (TIRF) microscopy, which allows imaging of a cell-bottom membrane with high signal-to-noise ratio, fluorochrome preservation, and

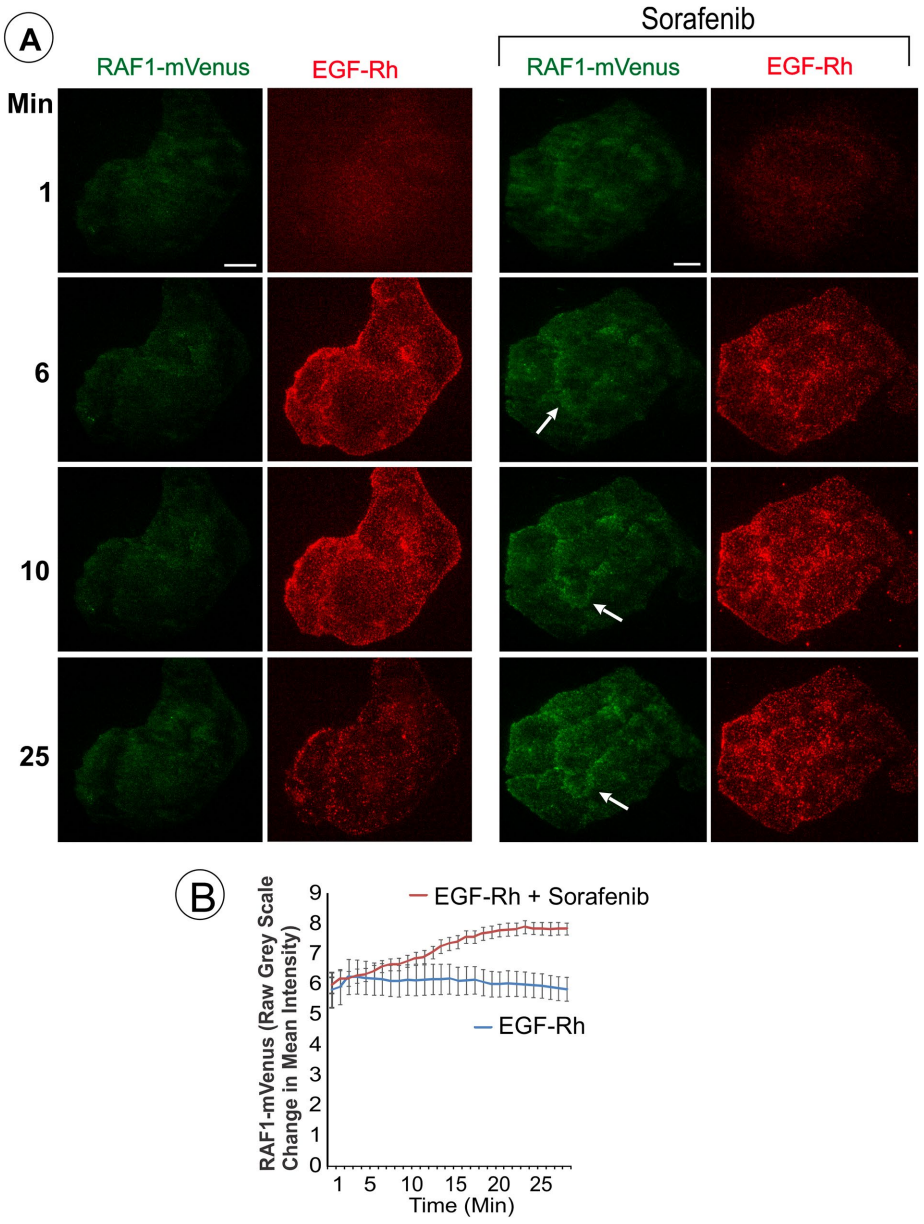


FIGURE 7: RAF1-mVenus is stabilized on the cell-bottom plasma membrane in cells treated with EGF in the presence of sorafenib. (A) HeLa/RAF1-mVenus cells were serum starved, and time-lapse TIRF imaging through 488- and 561-nm channels was performed during cell incubation with EGF-Rh (4 ng/ml) without and with sorafenib (10 μM) at 37°C. The arrows point out the example of the membrane RAF1-mVenus in cells treated with EGF-Rh and sorafenib. Scale bar, 10 μm. (B) Quantification of the fluorescence intensity of RAF1-mVenus in nine TIRF time-lapse image series exemplified in A.

resolution that are superior to those for confocal imaging. The high sensitivity of TIRF microscopy is evident from the detection of the persistent presence of EGF-Rh puncta for at least 30 min after cell stimulation (Figure 7A). The number of EGF-Rh puncta reached a maximum at 5 min of continuous incubation and gradually decreased for the subsequent 25 min of the time-course experiments. By contrast, under the same experimental conditions, confocal three-dimensional imaging detected very little, if any, EGF-Rh on the plasma membrane (Figures 2 and 4).

Time-lapse TIRF imaging of cells stimulated with EGF-Rh revealed weak diffuse mVenus fluorescence, which likely resulted from out-of-focus background fluorescence of the cytosolic mVenus (Figure 7A). The pattern did not change visibly during cell incubation with EGF-Rh. Membrane-like RAF1-mVenus localization was occasionally observed at early time points upon EGF-Rh stimulation (Figure 7A), but no statistically significant increase in the mean value of the fluorescence intensity was observed in multiple time-lapse sequences during early time-points of cell stimulation with EGF-Rh (Figure 7B). This observation suggests that RAF-mVenus transiently translocates largely to the ventral rather than the dorsal membrane of the cell, as also evident in Figures 2A and 3A. Likewise, membrane RAF1-mVenus was not detected at later incubation times. A combination of EGF-Rh and sorafenib, however, led to a clearly distinguishable accumulation of RAF1-mVenus on the dorsal cell membrane (Figure 7, A and B). No colocalization of punctate EGF-Rh and RAF1-mVenus fluorescence was observed. Given the high sensitivity of TIRF imaging, these experiments suggest that the residence time of RAF-mVenus on the cell-bottom membrane in EGF-stimulated cells is extremely short, resulting in the lack of a detectable pool of RAF1-mVenus on this membrane unless the membrane association of RAF1 is stabilized by sorafenib.

### Membrane translocation of RAF1 measured by subcellular fractionation

Fluorescence microscopic imaging demonstrated transient plasma membrane translocation of RAF1-mVenus upon cell stimulation with EGF but increased membrane priming of RAF1-mVenus in the presence of sorafenib. To examine the relationship between RAF1 membrane localization and its phosphorylation, the amounts of phosphorylated (pS338) and total RAF1-mVenus were measured by Western blotting in the cytosol and the membrane fraction of cells treated with EGF alone or together with sorafenib. Under all conditions, the membrane fraction of RAF1-mVenus was less than 0.05–0.1% of the total cellular RAF1-mVenus (Figure 8B). The percentage of membrane RAF1-mVenus phosphorylated at Ser338 (pS338RAF1) to total RAF1-mVenus was higher (up to 2.5%), indicating that a relatively higher proportion of active Raf1 is present on the membrane than in the cytosol. A trend of a small increase in the membrane fraction of RAF1-mVenus was observed after 5 min of cell treatment with EGF, although this increase was not statistically significant. The largest amount of RAF1-mVenus in the membrane fraction was observed after 15 min of cell stimulation with EGF in the presence of sorafenib (Figure 8C). Western blot analysis also showed that sorafenib alone did not affect the localization or phosphorylation of RAF1. Essentially similar results were obtained by subcellular fractionation of parental HeLa cells (unpublished data). Interestingly, sorafenib inhibition of MEK1/2

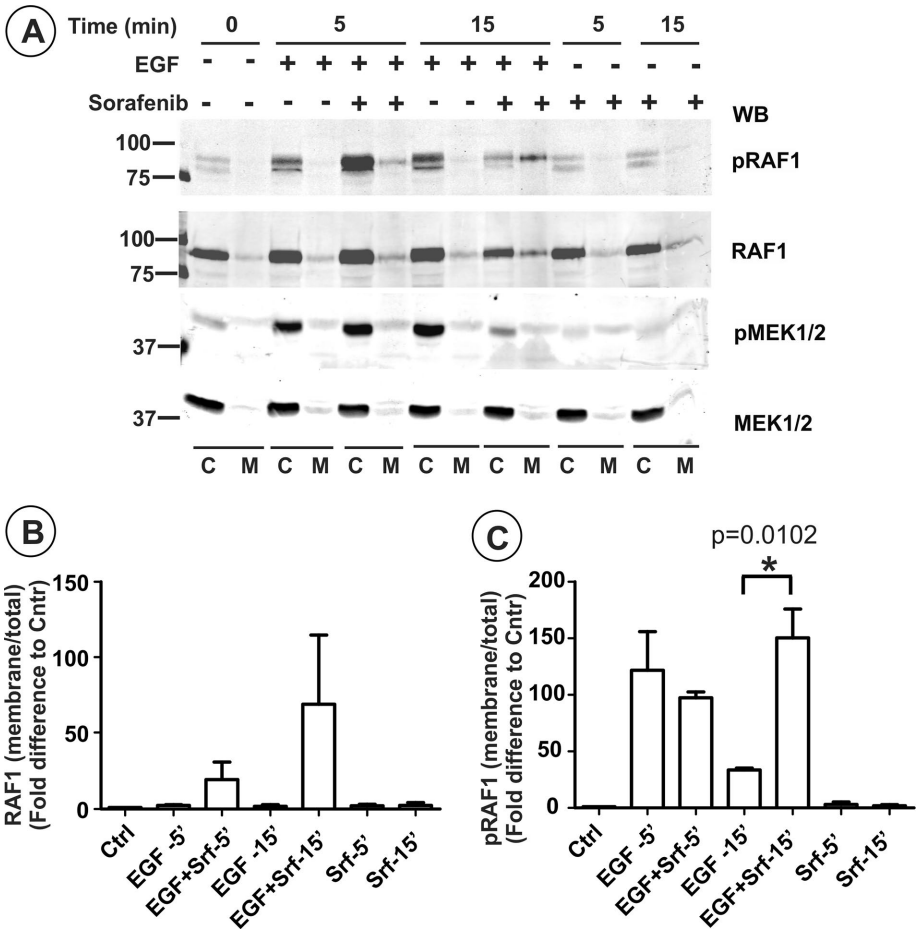


FIGURE 8: Subcellular fractionation of RAF1-mVenus in EGF- and sorafenib-treated cells. (A) HeLa/RAF1-mVenus cells were serum starved and incubated with EGF (4 ng/ml) (EGF) alone, sorafenib (Srf) alone, or combined EGF and sorafenib (EGF+Srf) for 0, 5, or 15 min at 37°C. At the end of incubation, cells were homogenized, and the membranes were separated from the cytosol by centrifugation. Total and phospho RAF1 (pSer338), and MEK1/2 were detected in cytoplasmic (C) or membrane (M) fractions by Western blotting. (B, C) Bar graphs represent mean values (±SEM) of the ratio of the amounts of pRAF1 and RAF1 in the membrane fraction to the amounts of total cellular (membrane plus cytosol) pRAF1 and RAF1, respectively, obtained from three independent experiments. Statistical significance was analyzed using unpaired Student's *t* test. $*p < 0.05$.

phosphorylation was not observed after 5 min of incubation with the inhibitor, when the membrane-stabilizing effect of sorafenib on RAF1-mVenus was already evident (Figure 8A). Both phosphorylated and nonphosphorylated MEK1/2 were detected only in cytoplasmic fractions. Overall, these biochemical measurements confirmed the conclusions of fluorescence imaging experiments, demonstrating that most RAF1, either active or inactive, is present in the cytoplasm, while sustained EGF-induced translocation of RAF1 to the membrane could be observed only in the presence of EGF and sorafenib.

### Computational modeling of RAF localization dynamics

To identify the key rate processes controlling the presence of RAF1 at the plasma membrane, a computational model of RAF1 dynamics was developed. The model was based mainly on mass action kinetic equations, with specific protein complexes accounted for based on published observations of the relative importance of hetero- and homodimers of particular RAF isoforms, and utilizing previously reported values for rate constants and protein expression as much as possible (*Materials and Methods*). RAS-GTP dynamics was fitted to our previously reported RAS kinetic measurements (Pinilla-Macua *et al.*, 2016) to avoid the need to consider upstream signaling processes and thus simplify the model (Supplemental Figure S5A). Our initial model failed to recapitulate experimentally observed RAF1 localization dynamics accurately during the first few minutes of EGF treatment (Figure 9A), showing almost no localization of RAF1 to the membrane. A univariate model sensitivity analysis revealed that the rate constants for RAF1 association and dissociation from RAS-GTP exerted the strongest control over predicted membrane RAF1 levels, and that RAS-GTP and RAF1 concentrations exerted the next strongest control (Figure 9B). For the initial model parameterization, RAF1 binding constants were based on measurements of RAS-GTP binding to immobilized recombinant RAF1 (Fischer *et al.*, 2007), which may not characterize binding in the cell physiological context realistically. By fitting the RAF1:RAS-GTP binding parameters, a model was obtained that recapitulated observed RAF1 membrane dynamics much more accurately (Figure 9A). To achieve good model agreement with data for sorafenib treatment, RAF1 binding constants in the presence of sorafenib were also refitted. Sensitivity analysis of the reparameterized models revealed that the parameters exhibiting the strongest control over model output remained unchanged, even with the addition of sorafenib (Figure 9B). The apparent binding affinity of inhibited RAF1 for RAS-GTP, based on the fitted parameters, was ~26-fold higher than that for uninhibited RAF1 (Supplemental Table S1), consistent with our observation that sorafenib stabilizes RAF1:GTP-RAS interactions at the membrane. To strengthen our conclusions, a more robust multivariate sensitivity analysis was undertaken using partial least-squares regression (PLSR). Random perturbations to all parameters were made simultaneously in numerous individual model runs, and regression of these random parameter sets was performed against the vector of predicted model outputs, resulting in $Q^2Y$ values of 0.45 and 0.40 for PLSR calculations with maximum or average membrane RAF1, respectively. This confirmed that the association and dissociation rate constants for RAF1:RAS-GTP binding and concentrations of RAS-GTP and RAF1 were the dominant parameters controlling predicted RAF1 membrane concentration, even when simultaneous changes to multiple parameters were considered (Figure 9C). Interestingly, a larger-than-expected number of observations were required to reach a conclusion using the PLSR-based approach due to the completely random nature of the model perturbations (Supplemental Figure S5B).

The validity of the trained model was probed by testing its ability to predict data not used for parameter fitting. Model simulations of the effects of increased RAS expression or of a constitutively active RAS mutant predicted that a higher fraction of RAF1 would remain

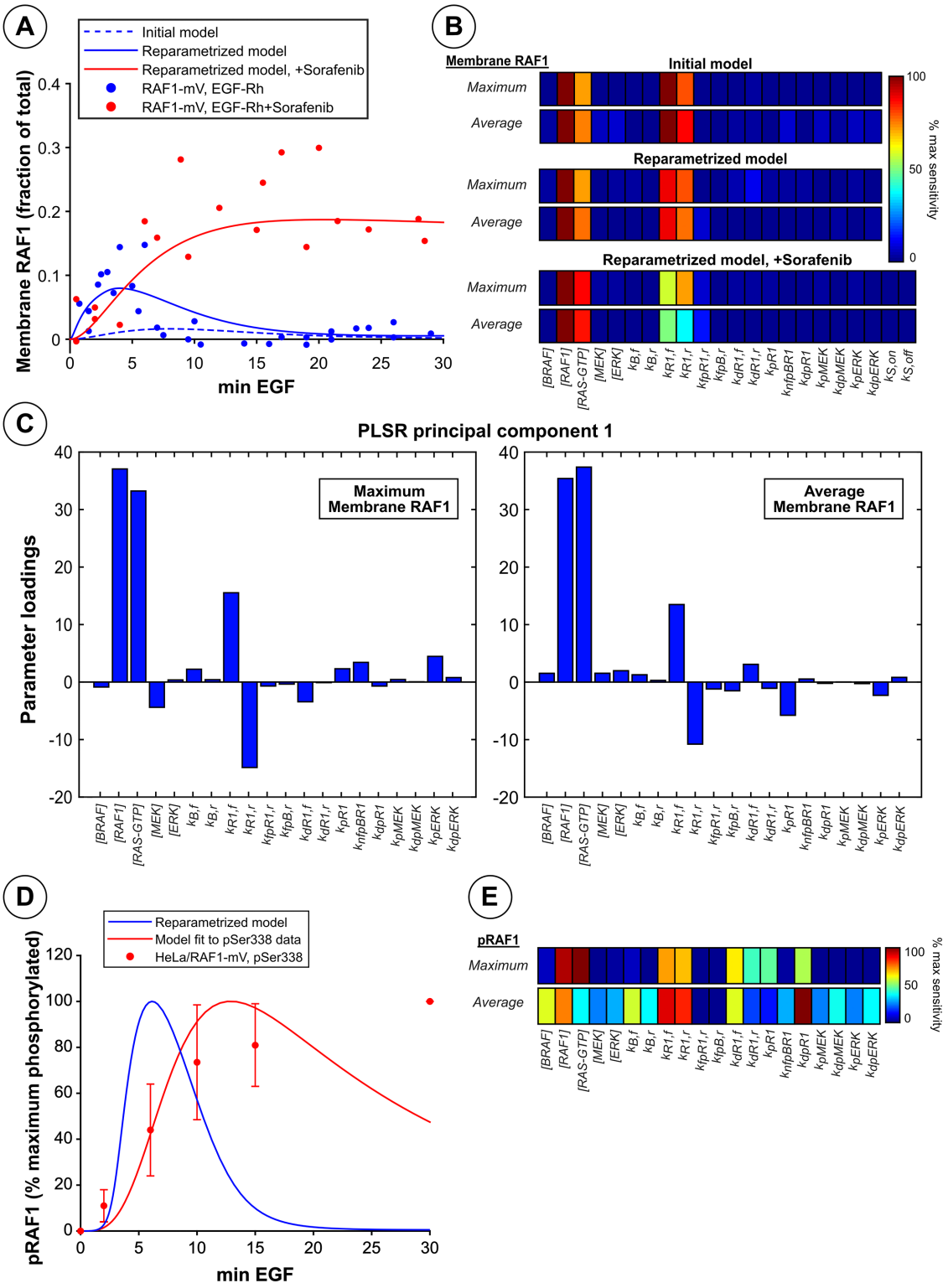


FIGURE 9: Computational model predictions and parameter sensitivity analysis for RAF1 membrane localization. (A) Model predictions (lines) for the fraction of membrane-bound RAF1 were compared with experimental results (points) from time-course imaging of HeLa/RAF1-mVenus cells during the first 30 min (from Figure 6B) of the response to 4 ng/ml EGF-Rh treatment with (red) or without (blue) sorafenib. (B) Sensitivity of model predictions for the maximum or average number of RAF1 molecules bound to RAS-GTP at the plasma membrane during the first 30 min of EGF treatment, with or without 10 μM sorafenib, to 10-fold changes in individual model parameters was calculated. For model predictions with sorafenib, $k_{R1f}$, $k_{R1r}$, $k_{B,f}$, and $k_{B,r}$ represent perturbations to the inhibited RAF1 and BRAF binding constants. (C) Multivariate model sensitivity analysis for 3000 random model parameter sets was performed by partial least-squares regression of parameter sets against the predicted maximum (left) and average (right) number of membrane-bound RAF1 molecules per cell in response to 30 min of 4 ng/ml EGF treatment. Loadings of individual

membrane-bound in each case, consistent with our experiments with overexpressed CFP-HRAS or CFP-HRAS-G12V (Supplemental Figure S5C). Increasing the concentration of RAF1 also resulted in increased RAF1 membrane localization in response to EGF, consistent with our observations of RAF1-YFP overexpression in HeLa cells (Supplemental Figure S5D). Simulations of EGF pretreatment followed by 20 min of 10 μM sorafenib treatment resulted in increased predicted RAF1 translocation to the membrane even after 30–60 min of stimulation with EGF (Supplemental Figure S5E), which is qualitatively consistent with experimental observations (Figure 5D).

With some confidence in the ability of the model to predict RAF1 membrane localization, we probed the model for insights into the central, unexpected observation of this study, namely that a relatively brief and small pulse of RAF1 membrane localization is apparently sufficient for sustained ERK activity over a substantially longer time scale. Given that observed pRAF1 kinetics was also more sustained than RAF1 membrane localization, and may therefore explain the downstream effects on ERK, we focused our analysis on factors controlling pRAF1 kinetics. Our first observation was that our trained model did not recapitulate observed pRAF1 dynamics well (Figure 9D), a consequence of the fact that RAF1 phosphorylation was not assumed to play a direct role in determining RAF1 membrane localization. To recapitulate observed pRAF1 kinetics reasonably well, we first performed a sensitivity analysis on the model prediction of total cellular pRAF1 (Figure 9E). The analysis identified four parameters, $k_{pR1}$, $k_{dpR1}$, $k_{dR1,f}$, and $k_{dR1,r}$, that most strongly controlled both the maximum and average levels of pRAF1. We fitted the model to experimental measurements of pSer338 in HeLa/RAF1-mVenus cells by allowing those parameters to vary by no more than a factor of 10 from their original values. The fitting resulted in fold changes of 1.05, 0.1, 0,48, and 3.26 for $k_{pR1}$, $k_{dpR1}$, $k_{dR1,f}$, and $k_{dR1,r}$, respectively, from their base values in the trained model (Supplemental Table S1). Applying these parameter changes to the model resulted in a more accurate prediction of pRAF1 kinetics (Figure 9D). The failure of the model to capture pRAF1 values well at the latest time point may be the result of transcriptional or translational processes not accounted for in our model. We note too that, with larger variations in the four parameters mentioned above permitted, the model can recapitulate pRAF1 dynamics well, even at the latest time point. However, such parameter sets suggest a rate of RAF1 deactivation that seems unrealistically small. Changes to key model parameters by less than an order of magnitude each led to a model that reasonably recapitulated observed pRAF1 kinetics, at least for $t \leq 15$ min, which is well past the observed peak in membrane association of RAF1. Given the way the signaling pathway is encoded computationally, our refitted model suggests that it is conceivable that the relatively small burst of RAF1 membrane localization is potentially consistent with observed ERK activation dynamics because, after the initial burst, RAF1 can continually rebind to active RAS at the membrane and undergo repeated rounds of reactivation many times over the course of signaling in response to EGF.

## DISCUSSION

In the present study, we employed gene editing to label endogenous RAF1 with mVenus fluorescent protein and analyzed localization of endogenous RAF1 in living HeLa cells stimulated with EGF. The main challenge of such an analysis is low abundance of RAF1 in the cell, requiring "extreme" image acquisition conditions. Recent mass-spectrometry measurements using labeled standard peptides demonstrated that RAF1 is expressed in ~12,000–14,000 copies per cell across various cell lines (Shi *et al.*, 2016). The predominantly diffuse distribution of RAF1 throughout the cytoplasm further complicates fluorescence microscopy imaging due to low signal-to-noise ratio. Low abundance of RAF1 also makes it difficult to examine the presence of RAF1 in endosomes due to interference by the autofluorescence in these compartments, which is unavoidably observed under the image acquisition conditions necessary to detect RAF1-mVenus. Using a simplified modification of the spectrum-unmixing approach to measure the nonspecific component of the fluorescence through the 515-nm channel, which corresponds to the autofluorescence of endolysosomal compartments, we demonstrated that RAF1-mVenus is not present in endosomes containing ligand–EGFR complexes (Figure 2). The experiments with sorafenib confirmed that even under conditions of stabilization of RAF1 on the membrane, the endosomal pool of RAF1-mVenus is undetectable (Figure 5). Interestingly, despite accumulation of constitutively GTP-loaded HRAS mutant on intracellular membranes, very little RAF1-mVenus was detected in these vesicles (Figure 4B). This observation implies that in addition to GTP-RAS, RAF binding to the membrane may require interaction with the components that are not available on endosomal membranes.

The lack of detectable endosomal RAF1-mVenus in HeLa cells is consistent with our earlier observation that endogenous HRAS is not present in endosomes containing EGFR in the same cells (Pinilla-Macua *et al.*, 2016). Previous studies including using overexpressed labeled RAF1 also did not demonstrate endosomal localization of RAF1 (Bondeva *et al.*, 2002). There are, however, observations of the endosomal localization of RAF in fixed Rat-1 cells by immunofluorescence and PC12 cells by subcellular fractionation (Rizzo *et al.*, 2000; Howe *et al.*, 2001). Certainly, the presence of a very small number of RAF1-mVenus molecules in endosomes is not ruled out, because of the limited sensitivity of the confocal imaging due to a low signal-to-noise ratio. Based on the minimal threshold of RAF1-mVenus detection of 2–3 molecules per endosome (Supplemental Figure S3) and having 30.9 ± 4.3 (SD) EGF-Rh–containing endosomes per cell as quantified from multiple three-dimensional images of cells stimulated with EGF-Rh for 10–15 min, it could be predicted that ~60–90 molecules of RAF1-mVenus could be present in endosomes but not detected in our measurements. However, together with the data demonstrating that RAS is not present in EGFR-containing endosomes in HeLa cells (Pinilla-Macua *et al.*, 2016) and our earlier demonstration of the lack of activated MEK2 in endosomes in the same cells (Galperin and Sorkin, 2008), the present study of RAF1 localization suggests that endosomes do not significantly contribute to the activation of MEK1/2 by RAF.

parameters into the first principal component of the PLSR model are shown. The overall PLSR $Q^2Y$ values with 10-fold cross-validation were ~0.453 and 0.401, respectively, for PLSR calculations with maximum and average membrane RAF1. The $Q^2Y$ values for the first principal components shown here were also ~0.451 and 0.397. (D) Predictions with the trained model were made for total cellular pRAF1 before (solid blue line) and after (solid red line) refitting four model parameters ($k_{pR1}$, $k_{dpR1}$, $k_{dR1,f}$, and $k_{dR1,r}$) to the observed dynamics of pSer338 in HeLa/RAF1-mVenus cells (red dots; see data in Figure 1D). All pRAF1 values were normalized to the maximum value within each respective data set. (E) Sensitivity of reparameterized model predictions for the maximum or average number of pRAF1 molecules per cell during the first 30 min of EGF treatment without sorafenib to 10-fold changes in individual model parameters was calculated.

While the absence of RAF1 in endosomes in our experimental system may not be surprising, EGF-dependent translocation of RAF1 to the plasma membrane was demonstrated in numerous studies (e.g., Stokoe *et al.*, 1994; Roy *et al.*, 1998) and was anticipated to be readily detectable. The observation of rather small amounts of RAF1-mVenus transiently associated with the plasma membranes and the lack of detectable sustained membrane association of RAF1-mVenus in EGF-stimulated cells were unexpected. It is well established that the kinase of RAF proteins is activated through the interaction with the membrane-associated GTP-loaded RAS. In conjunction with such a view, in our experiments the peak of RAF1-mVenus translocation to the plasma membrane was observed at the same time as the peak of RAS activity in these cells (Figure 3B; Pinilla-Macua *et al.*, 2016), which is consistent with the model sensitivity analysis, suggesting that the concentration of RAS-GTP controls the membrane pool of RAF1 (Figure 9). However, the relative size of the membrane pool of RAF1-mVenus was not increased when the constitutively active RAS mutant was overexpressed as compared with the same pool in EGF-stimulated, wild-type RAS-overexpressing cells (Figure 4C), suggesting that the amount of GTP-RAS is not the only limiting factor for the membrane binding of RAF1, as also suggested by the modeling (Figure 9). Interestingly, membrane translocation of RAF1-mVenus was more readily detected in a larger pool of cells if cells were not serum-starved before EGF stimulation than with the serum-starved cells (Supplemental Figure S6), suggesting that signaling via mechanisms in addition to those by EGFR may prime/augment RAF1 membrane translocation.

The experiments with sorafenib confirmed that when RAF1 membrane priming is stabilized, endogenous labeled RAF1 is readily detectable by confocal or TIRF imaging on the plasma membrane. The mechanism of this effect of sorafenib is not fully understood. It has been suggested that binding of RAF kinase inhibitors unlocks an autoinhibitory conformation of RAF proteins, thus increasing RAF binding affinity to RAS-GTP, and/or stabilizes RAF1 homodimers and RAF1:BRAF heterodimers, thus leading to increased avidity of the interaction with GTP-RAS (Poulikakos *et al.*, 2010; Jin *et al.*, 2017). Sorafenib did not increase membrane association of transiently expressed RAS binding domain (RBD) of RAF or a larger construct including the RBD and cysteine-rich domain of RAF1 (Bondeva *et al.*, 2002) in cells stimulated with EGF (unpublished data), suggesting that the RAF kinase domain may be important for sorafenib effects. Sensitivity analysis performed on our computational model suggested that the RAF1 membrane pool is primarily controlled by RAF1's affinity for GTP-loaded RAS rather than by RAF dimerization parameters (Figure 9, B and C). Another factor that is thought to be involved in the release of RAF from the membrane is a feedback negative regulation through phosphorylation of RAF by ERK1/2 leading to RAF kinase deactivation and dissociation from the membrane (Lake *et al.*, 2016). However, the effect of MEK1/2 inhibitors on the membrane association of RAF1 was substantially smaller and significantly delayed as compared with those effects of sorafenib (Hatzivassiliou *et al.*, 2010; also unpublished data). We further note that this ERK-regulated feedback effect was included in our model, but that it had little effect on predicted RAF1 membrane localization (unpublished data). Finally, it is possible that low concentration of BRAF is a parameter limiting the membrane pool of RAF1, given that RAF1:BRAF heterodimers were shown to be the main dimer species in HeLa cells (Freeman *et al.*, 2013). However, membrane concentration of RAF1 was not sensitive to BRAF levels in modeling analysis (Figure 9), and overexpression of BRAF did not increase the membrane translocation of RAF1-mVenus in our experiments (Supplemental Figure S7). Thus, it is most plausible that the increased affinity of RAF1:GTP-RAS interaction in the presence of sorafenib could be the main mechanism that prevents rapid release of RAF1 from the membrane. The most likely interpretation of highly transient membrane association of RAF1 in the absence of sorafenib is that RAF1 is recruited to the plasma membrane through binding to GTP-RAS and possibly another lipid-dependent interaction, which leads to activation of the RAF kinase and is followed by rapid kinase inactivation and release of RAF from GTP-RAS into the cytosol. Such highly dynamic RAF1 translocation results in an extremely low concentration of RAF1 on the plasma membrane following an initial translocation peak after EGF stimulation, precluding detection of the membrane pool of RAF1-mVenus by fluorescence microscopy and subcellular fractionation in cells incubated with EGF for more than 6–8 min.

Regardless of the regulatory mechanisms underlying RAF membrane translocation, a small membrane pool of RAF1 and its transient membrane residence appear to be sufficient for the sustained downstream signaling. Because RAF1-mVenus may be considered as the sensor of RAS-GTP, "sorafenib" experiments (Figure 5) imply that a pool of RAS-GTP is present in the plasma membrane for an extended period of time during EGF stimulation. These observations further confirm that the inability to detect sustained membrane localization of RAF1-mVenus is likely due to highly transient interaction with the membrane rather than the lack of GTP-RAS at the plasma membrane. On the other hand, it is possible that stabilization of RAS-RAF interaction by sorafenib protects RAS from GTP hydrolysis by RAS GTPase–activating proteins, and therefore, the amount of GTP-loaded RAS in sorafenib-treated cells may be overestimated as compared with that in control cells. Furthermore, it should be noted that subcellular fractionation could not be used to measure the fraction of membrane RAF1-mVenus because RAF1 appears to dissociate from the membrane during cell homogenization and centrifugation (Figure 8). By contrast, imaging of intact cells allowed estimation of the number of RAF1-mVenus molecules on the plasma membrane (Figures 3B and 5B), which yielded a maximum number of RAF1-mVenus on the plasma membrane of ~1200–1800 per cell at the peak of translocation. ARAF is typically expressed at similar or slightly higher levels than RAF1 (Shi *et al.*, 2016). Although ARAF does not appear to play a significant role in signaling to ERK1/2 in HeLa cells (Freeman *et al.*, 2013), it is possible that at the peak of the translocation, the total amount of RAF proteins on the plasma membrane is twice as high as that of RAF1, or roughly 4000 per cell. Projecting that the "after-peak" RAF1 membrane concentration is <10% of its highest membrane concentration at early time points of EGF stimulation (based on the time course of RAS-GTP concentration), at maximum 180 RAF1 and 400 total RAF molecules per cell are present on the membrane after 6–8 min of EGFR activation. Remarkably, such a small membrane pool of RAF1 appears to be sufficient for sustaining MEK1/2 and ERK1/2 activities that decay significantly only after 30–45 min of EGF stimulation (Figure 1). An alternative possibility is that a significant fraction of RAF1 remains active in the cytosol after dissociation from the membrane, and this large pool of RAF is responsible for phosphorylation of MEK1/2 and sustained ERK1/2 activity. But this possibility is not supported, to our knowledge, by experimental evidence.

Finally, we note that the conclusions of our computational model are subject to certain limitations, including our ability to parameterize the model properly and to identify and encode the most critical protein–protein interactions among all possible interactions that potentially regulate RAF1 dynamics. A common issue in mechanistic models of this kind is the combinatorial explosion of species that

occurs when multiple phosphorylation sites are considered on individual proteins. This issue tends to lead investigators to lump phosphorlylation and kinase activation processes into a smaller number of modeled protein modifications than explain the known biology. As long as those reductionist choices capture the most relevant processes, however, such models can still provide physical insight. Indeed, this was indicated by our finding, mentioned above, that consideration of the effect of ERK-regulated feedback on RAF1 membrane binding did not change our central model conclusions.

## MATERIALS AND METHODS

### Reagents

Recombinant human EGF was purchased from BD Biosciences; EGF-Rh was from Molecular Probes (Invitrogen). Mouse monoclonal antibody to RAF1 was obtained from BD Transduction Laboratories (San Jose, CA). Rabbit monoclonal antibody to pSer338 RAF1, monoclonal antibody to MEK1/2, ERK1/2, polyclonal rabbit antibodies to phosphorylated MEK1/2, phosphorylated ERK1/2, and α-actinin were from Cell Signaling Technology (Danvers, MA). Secondary anti-mouse and anti-rabbit IRDye antibodies were from Li-COR. Sorafenib was purchased from Santa Cruz and stored as 10 mM stock solution in dimethyl sulfoxide (DMSO) at −20°C. CellMask, PCR, cloning, and other reagents and chemicals were from Thermo Fisher (Pittsburgh, PA).

### Generation of gene-edited HeLa/RAF1-mVenus cells by CRISPR-Cas9

gRNAs for human *RAF1* were designed using online algorithms based on the highest on-target score and distance from the stop codon of *RAF1*. Oligos for gRNA were obtained from Thermo Scientific: *RAF1*-sgRNA-3F 5′CACCGCACG CTGACCACGTCCCCG 3′ and RAF1-sgRNA-3R 5′ AAACCGGGGACGTG GTCAGCGTGC 3′. The oligos were annealed in vitro and cloned in pSpCas9(PX330) and pSpCas9(BB)-2A-Puro (PX459) plasmids (gifts from Feng Zhang, Broad Institute, Cambridge, MA; Ran *et al.*, 2013) using the *Bbs*I cloning site for the expression of gRNA and Cas9. Donor vectors were generated by cloning mVenus sequence flanked by ~1 kb left and right homology arms from the *RAF1* stop codon in the pUC18 plasmid. Point mutations were generated in the sgRNA target sequence in the donor DNA sequence without altering the reading frame of *RAF1*, so that the repaired strand is not recut by Cas9 after transfection. A linker of 27 bases corresponding to nine amino acids was also added before the start codon of mVenus. The donor vector was confirmed by digestion and sequencing.

HeLa cells were transfected with gRNA-containing plasmids pSpCas9(PX330 (0.3 μg) or pSpCas9(BB)-2A-Puro (PX459) and donor plasmid (0.6 μg) using Effectene transfection reagent (Qiagen) per the manufacturer's protocol. The medium was changed after 24 h. Genomic DNA from untransfected and transfected HeLa cells was isolated using a Wizard Genomic DNA purification kit (Promega) per the manufacturer's instructions. Genomic DNA (200 ng) was used to amplify the region around the *RAF1* stop codon using Phusion HF DNA polymerase (Thermo Fisher) and primers F-5′ GAGCATTCTTGGGCTTTGTTT 3′ and R-5′ ATGAAGTTAAGGCCCTGTGAG 3′. The expected size of products from WT gDNA was 320 base pairs and of products from homozygous RAF1-mVenus gDNA was 1066 base pairs. The PCR products were confirmed by electrophoresis and sequencing. The first round of transfection resulted in HeLa clones with the insertion of mVenus into one allele of *RAF1*, as confirmed by PCR and Western blot analysis. The clones were obtained by single-cell clone isolation. The second round of transfection in the clone carrying the single-allele *RAF1*-mVenus cells with pSpCas9(BB)-2A-Puro (PX459) -RAF1 sgRNA#3 and donor vector resulted in a clone with mVenus inserted into both alleles of the *RAF1* gene. The insertion in this clone was confirmed by PCR and Western blotting. The resulting clone is referred to as "HeLa/RAF1-mVenus cells."

### DNA constructs and cell transfection

EGFR-YFP was previously described in Sorkin *et al.* (2000). RAF1-YFP, CFP-HRAS, and CFP-HRASG12V mutant constructs were also described previously (Jiang and Sorkin, 2002). DNA plasmids were transfected using Lipofectamine or Effectine according to the manufacturer's instructions. TagRFP-BRAF was prepared by cloning the full-length sequence of human BRAF into the pTagRFP-C1 vector. The full-length BRAF sequence was amplified from pCDNA-BRAF plasmid, a gift from Dustin Maly (University of Washington, Seattle; Addgene plasmid #40775), using primers with *Hin*dIII and *Pst*I restriction sites at the 5′ and 3′ ends of BRAF ORF, respectively. The amplified product was digested by *Hin*dIII and *Pst*I and cloned into pTagRFP-C1 plasmid digested with the same restriction enzymes. The resulting pTagRFP-BRAF plasmid was confirmed by digestion and sequencing.

### Cell culture

HeLa and HeLa/RAF1-mVenus cells were cultured in DMEM supplemented with 10% FBS. HeLa cells constitutively expressing Grb2-YFP in the absence of endogenous Grb2 were maintained as described previously (Huang and Sorkin, 2005; Fortian and Sorkin, 2014). The identity of parental HeLa cells was confirmed by STR profiling. The cells are regularly tested for mycoplasma contamination.

### Live-cell confocal microscopy

The cells were grown in MatTek dishes (MatTek Corporation, Ashland, MA). Live-cell imaging was performed at 37°C using a spinning-disk confocal Marianas system based on a Zeiss Axio Observer Z1 inverted fluorescence microscope equipped with 405-, 445-, 488-, 515-, 561-, and 640-nm lasers, 63× oil immersion objective, EM-CCD camera, piezocontrolled *z*-step motor. and temperature-controlled environmental chamber to maintain 37°C and 5% $CO_2$, all controlled by Slidebook 6 Software (Intelligent Imaging Innovation, Denver, CO). Typically, a *z*-stack of 15 images was acquired at 400-nm steps.

### Image analysis

To estimate colocalization of EGF-Rh and RAF1-mVenus in endosomes, parental HeLa and HeLa/RAF1-mVenus cells were incubated with 4 ng/ml EGF-Rh for 10–30 min. At that time, the EGF-Rh fluorescence signal was predominantly detected in endosomes. Cells not stimulated or stimulated with EGF-Rh were imaged through 445-, 515-, and 561-nm channels using identical image acquisition parameters. Segment Mask #1 was generated from three-dimensional images to select vesicles using a minimal threshold of the vesicular 561-channel fluorescence intensity. This threshold was kept identical in images of cells that were not exposed to EGF-Rh (autofluorescence through the 561-nm channel) and cells incubated with EGF-Rh (rhodamine fluorescence plus autofluorescence). Objects smaller than 16 voxels were eliminated from Mask #1. The background Mask #2 was generated by dilating each object in Mask #1 by two voxels in three dimensions. The mean fluorescence intensities in each three channels of Mask #2 (voxels surrounding all objects in Mask #1) were subtracted from those intensities of Mask #1 to obtain mean specific intensities of vesicular compartments in

individual images ($I^{445}$, $I^{515}$, and $I^{561}$). The mean ratio of $I^{515}$ and $I^{445}$ was first calculated from multiple images of parental cells to obtain a mean value of the autofluorescence correction coefficient ($k_{auto}$). $k_{auto}$ was used to calculate the autofluorescence component (auto$I^{515}$) of the $I^{515}$ values measured in RAF1-mVenus-expressing cells in each image containing multiple cells using the equation auto$I^{515} = k_{auto} \times I^{445}$. auto$I^{515}$ was then subtracted from $I^{515}$ to obtain a mean fluorescence intensity of mVenus (mV). Finally, the ratio of mV and $I^{561}$ ("mV/561") was calculated. Because the intensity of EGF-Rh fluorescence in endosomes was significantly higher that the autofluorescence of endosomes in the 561 channel, $I^{561}$ values were not corrected for autofluorescence. In control experiments, HeLa/Grb2-YFP and HeLa/EGFR-YFP cells stimulated with EGF-Rh were imaged through 561-, 515-, and 445-nm channels using the same parameters as in experiments with RAF-mVenus–expressing cells. Given that the fluorescence properties of YFP and mVenus are identical at the neutral pH of the cytosol, calculations of the YFP/561 fluorescence ratios were performed as described above for the mV/561 ratio.

To estimate the fraction of membrane-associated RAF1-mVenus in HeLa/RAF1-mVenus cells, the cells were stained with CellMask to label membranes and then treated with EGF-Rh alone or together with sorafenib and imaged through 640-nm (CellMask), 561-nm (rhodamine), and 515-nm (mVenus) channels. Three-dimensional images of CellMask were deconvolved using a no-neighbors algorithm. Mask#1 was generated to select all voxels containing mVenus (total mVenus). Voxels containing both CellMask and mVenus fluorescence were selected using the interactive segmentation tool of SlideBook 6 to generate Mask#2 (membrane mVenus). The sum intensity of background-subtracted Mask #2 was divided by the sum intensity of background-subtracted Mask #1 to obtain the fraction of RAF1-mVenus associated with the membrane. In the experiments with transient expression of CFP-HRAS or its mutant, measurements of the membrane fraction of RAF1-mVenus were performed using the CFP fluorescence as the membrane marker instead of the CellMask fluorescence.

To estimate the minimal threshold of the fluorescence intensity of mVenus or YFP that can be detected in endosomes in our imaging experiments, HeLa cells transiently expressing EGFR-YFP were stimulated with EGF-Rh (4 ng/ml) for 10–15 min at 37°C, and three-dimensional images were acquired using parameters identical to those used for imaging of RAF1-mVenus as described above. First, the value of the autofluorescence correction coefficient ($k_{auto}$) was calculated using three-dimensional images of nontransfected cells acquired through 445- and 515-nm channels and selecting individual endosomes using the 561-nm channel as described above. The apparent mean intensity of the fluorescence through the 515-nm channel (a.l.u.f.i. per voxel) was determined in individual endosomes containing EGF-Rh in cells not expressing EGFR-YFP or expressing the lowest visually detectable level of EGFR-YFP. The values of the mean intensity through the 515-nm channel in individual EGF-Rh–containing endosomes were corrected for autofluorescence determined using the above-calculated $k_{auto}$ to obtain values of the *specific* mean YFP intensity per voxel of individual endosomes. The number of EGF-Rh–containing endosomes per cell incubated with EGF-Rh for 10–15 min was determined by generating a segment mask using three-dimensional images acquired through the 561-nm channel and quantitating the number of objects in this mask per cell in multiple images.

To estimate the apparent fluorescence intensity corresponding to a single YFP or mVenus molecule, total fluorescence intensity of mVenus per HeLa/RAF1-mVenus cell was calculated using three-dimensional imaging through the 515-nm channel in multiple cells. The mean value of mVenus intensity per cell was divided by the number of RAF1 molecules per cell (12,000; see Supplemental Table S1) to yield the value of the mean intensity of 16,147 ± 2100 (SEM) a.l.u.f.i. per single RAF1-mVenus molecule.

To estimate the minimal threshold of mVenus detection using an additional approach, HeLa/RAF1-mVenus cells were prestained with CellMask, stimulated with EGF for 2–5 min, and imaged as described above. First, voxels containing membrane RAF1-mVenus were selected using CellMask-based segmentation (Mask #1). Second, the background Mask#2 was generated by selecting voxels surrounding individual objects within Mask #1 larger than 10 voxels with an apparent concentration of RAF1-mVenus (ruffles, protrusions) over the diffuse cytosolic mVenus fluorescence. Third, the specific mean fluorescence intensity of individual objects containing membrane-associated RAF1-mVenus was calculated by subtracting background (Mask #2) from individual objects in Mask #1.

### TIRF microscopy

Time-lapse TIRF microscopy imaging of serum-starved HeLa/RAF1-mVenus cells was performed before and during EGF-Rh stimulation in the absence or presence of sorafenib using Nikon Eclipse Ti inverted microscope (Nikon), 100×, 1.49 N.A. oil-immersion objective, Photometrics 95B camera, through 488-nm (mVenus) and 561-nm (EGF-Rh) channels at 37°C. Image analysis was performed using Nikon Elements Software. Total cell-associated intensities of mVenus and rhodamine fluorescence were quantitated for each *x*–*y* image position. Mean values of the background-subtracted fluorescence intensities of multiple *x*–*y* images were calculated at each time point and plotted against time.

### Subcellular fractionation

Parental HeLa and HeLa/RAF1-mVenus cells grown in 10-cm dishes were treated with EGF (4 ng/ml) or sorafenib (10 μM) or EGF plus sorafenib for 0, 5, or 15 min. After treatment, the cells were washed with ice-cold PBS. Thereafter all the steps were carried out at 4°C. The cells were scraped into a hypotonic buffer (Stokoe *et al.*, 1994) containing protease inhibitors and incubated for 15 min and then homogenized by being passed through a 27 G needle 10 times. Homogenates were rotated on a nutator for 20 min and spun at 2000 × *g* to remove cell debris, nuclei, and mitochondria. The supernatant was spun at 100,000 × *g* for 1 h to separate membranes from the cytosol fraction (supernatant). The pellet was washed with hypotonic buffer, and this membrane fraction was solubilized in the TGH buffer (1% Triton X-100, 10% [vol/vol] glycerol, 50 mM HEPES) containing EDTA, protease and phosphatase inhibitors, and 0.5% deoxycholate. The lysates of membrane fractions and the cytosol fractions were heat-denatured in the sample buffer. Samples were run on SDS–PAGE, transferred to nitrocellulose membranes, and probed by Western blotting as described (Pinilla-Macua *et al.*, 2016). The blots were imaged by Li-COR. Quantification of band intensities was performed using ImageJ. The total RAF1 and phosphoRAF1 were calculated as sums of cytoplasmic and membrane fractions. The fraction of membrane RAF1 was calculated as the percentage of total RAF1 in each experimental variant. The data were normalized to the percentage of membrane RAF1 signal in untreated cells.

### RAF1, MEK1/2, and ERK1/2 phosphorylation

Parental HeLa and HeLa/RAF1-mVenus cells were stimulated with 4 ng/ml EGF for the indicated times. Cells were lysed in TGH, and lysates were electrophoresed on 10% polyacrylamide gels. The blots were probed with antibodies against total and phosphorylated RAF1 (pS338), pMEK1/2, pERK1/2, MEK1/2, and ERK1/2. Blots

were imaged and quantified by Li-COR. Ratios of the amounts of phosphorylated protein to the amounts of total protein were calculated and are expressed as percentages of the maximum ratio in each time course.

### Model development and implementation

***Model overview.*** The computational model consists of a set of coupled ordinary differential equations that describe binding interactions and reaction kinetics among RAS, RAF1, BRAF, and sorafenib during the first hour of cell response to EGF binding. Model interactions and parameters are defined and listed in Supplemental Figure S8 and Supplemental Table S1. Model equations were generated and compiled using Virtual Cell (Vcell; Blinov *et al.*, 2017). In total, the model includes 36 distinct protein species and 40 reactions. Model calculations were made using MATLAB (Version 2017A) for all results shown by exporting the model from VCell as a MATLAB-compatible ODE function and solving the system of coupled equations using the solver *ode15s*. The VCell model, "Surve_et_al_RAF1," is available in the public domain at http://vcell.org/vcell-models under the shared username "pmyers1995."

***RAS-GTP dynamics.*** RAS-GTP dynamics was forced to follow a functional form (Supplemental Eq. S1) by fitting to the model output of total RAS-GTP previously reported experimental RAS activation kinetics (Pinilla-Macua *et al.*, 2016) using *fminsearchbnd* (constrained Nelder-Mead) in MATLAB (Supplemental Figure S5A). It was assumed that different RAS isoforms do not differ significantly in their binding affinities to RAF protomers and that they could all be described as a single RAS species in the model. All RAS molecules were assumed inactive at time $t = 0$. Based on measurements of total RAS isoforms in HeLa cells (total ~135,000 KRAS, HRAS, and NRAS molecules per cell; Shi *et al.*, 2016), there are ~20% GTP-loaded RAS of total RAS (our unpublished calculations based on the data in Pinilla-Macua *et al.*, 2016, and calculations based on Figure 1 in Omerovic *et al.*, 2008) and thus ~27,000 molecules per cell of RAS-GTP at maximum activation. Approximately 2–4000 molecules of GTP-RAS per cell are present after 15 min of EGF treatment (based on Pinilla-Macua *et al.*, 2016).

***RAF binding to RAS-GTP.*** RAF1 and BRAF bindings to active RAS-GTP at the plasma membrane were initially modeled as reversible processes with characteristic association and dissociation rate constants as measured previously (Fischer *et al.*, 2007). Refitting of the RAF1:RAS-GTP binding rate constants ($k_{R1,f}$ and $k_{R1,r}$) using experimental observations of the fraction of RAF1 localized to the membrane (Figure 6B) was performed using *fminsearchbnd* in MATLAB. The binding and unbinding of RAF1 phosphorylated on its activating site (pRAF1) from RAS-GTP was modeled as a reversible process with the same rate constants as inactive RAF1 binding and unbinding to RAS-GTP. The dissociation of RAF1 phosphorylated on its negative feedback site from RAS-GTP was modeled as a first-order, irreversible process using the initial rate constant of RAF1 unbinding from RAS (Fischer *et al.*, 2007) multiplied by 10 to account for observations that ERK-mediated phosphorylation of Raf disrupts RAS-RAF complexes (Lavoie and Therrien, 2015). The unbinding of feedback-inhibited BRAF from RAS-GTP was also modeled as first-order and irreversible, and the rate constant of BRAF unbinding from RAS was multiplied by 10 ($k_{fpB,r}$). Association and dissociation rate constants of sorafenib-inhibited RAF1 (iRAF1) with RAS-GTP ($k_{iR1,f}$ and $k_{iR1,r}$) and the dissociation rate constant ($k_{fpR1,r}$) of iRAF1 phosphorylated at the negative feedback site with RAS-GTP were also fitted to experimental observations of the fraction of RAF1 localized to the membrane during EGF stimulation in the presence of sorafenib. Thus, when sorafenib was included in model calculations, $k_{fpR1,r}$ was set to its fitted value, $4.9 \times 10^{-3}$ min$^{-1}$, for the dissociation reaction between nfpiRAF1 and RAS-GTP.

***RAF dimerization.*** RAF dimerization was modeled as a reversible process occurring at the plasma membrane between any RAS-bound BRAF and any RAS-bound RAF1 species that were not phosphorylated at their negative feedback sites; active, phosphorylated RAF1 (pRAF1) and inactive RAF1; two pRAF1 molecules; any two BRAF molecules that are not feedback phosphorylated; and two iRAF1 molecules. While other computational models accounting for RAF dimerization in response to RAS activation have been developed (Hibino *et al.*, 2011; Varga *et al.*, 2017), they described RAF dimerization kinetics as first-order processes, which renders their kinetic parameters inapplicable to the second-order descriptions of RAF dimerization used in our model. Accordingly, rate constants of RAF dimerization were approximated here assuming diffusional limitations (Lauffenburger and Linderman, 1996). The membrane diffusivity of RAS-GTP:RAF complexes was set to 0.2 $\mu m^2 \cdot s^{-1}$ (Lommerse *et al.*, 2005), and the interaction radius was set to 1 nm (Lauffenburger and Linderman, 1996). HeLa cells were approximated as spheres of radius 10 μm (Kholodenko, 2002). The number of RAS:RAF complexes present was set to $1.5 \times 10^3$/cell, based on our experimental measurements of maximal RAF1-mVenus membrane loading. The rate constant for RAF dimer dissociation was calculated assuming an equilibrium dissociation model and a dissociation constant of 770 nM for membrane-bound, GTP-loaded K-RAS dimers (Muratcioglu *et al.*, 2015).

BRAF:RAF1 dimers are the dominant heterodimer species formed in HeLa cells during EGF stimulation, contributing to elevated RAF1 kinase activity (Freeman *et al.*, 2013). ARAF:RAF1 heterodimer formation was thus not considered. There is also evidence that RAF1 monomers phosphorylated at S338 may serve as allosteric activators for other RAF1 monomers in a positive feedback interaction (Hu *et al.*, 2013). The model accounts for this by allowing RAF1 homodimers to form from pRAF1:RAS-GTP and RAF1:RAS-GTP species. RAF kinase inhibitors stimulate RAF dimer formation by stabilizing an open conformation of RAF kinases at the plasma membrane (Hatzivassiliou *et al.*, 2010; Poulikakos *et al.*, 2010; Lavoie *et al.*, 2013). The model allows the reversible formation of iBRAF:RAF1, BRAF:iRAF1, and iRAF1:iRAF1 dimer species based on these observations.

***RAF1, MEK, and ERK phosphorylation.*** The regulation of RAF1 by phosphorylation is complex and involves multiple phosphorylation sites and kinases that control RAF1's catalytic activity (Lavoie and Therrien, 2015). We simplified the model's description by assuming that RAF1 activating phosphorylation occurs on a single residue. This was implemented by modeling RAF1 phosphorylation at the membrane as an irreversible, first-order process using a rate constant for RAF phosphorylation, as in a previous model of ErbB signaling (Chen *et al.*, 2009). Cytoplasmic pRAF1 is dephosphorylated by protein phosphatases, thus deactivating it and regenerating the initial RAF1 species. This interaction was modeled as zeroth-order with respect to protein phosphatases. The rate constant for pRAF1 dephosphorylation was approximated with a nominal rate constant for dephosphorylation, as previously described (Chen *et al.*, 2009). Feedback phosphorylation of RAF1, iRAF1, BRAF, and

iBRAF by active ERK at a single site was modeled as an irreversible, second-order process using a rate constant ($k_{nfpBR1}$), as described in a previous model of RAF activation (Varga *et al.*, 2017). MEK phosphorylation was modeled as second-order, irreversible, and catalyzed by any species containing pRAF1 or dimerized and uninhibited BRAF using a rate constant from the same previous model of RAF activation (Varga *et al.*, 2017). ERK phosphorylation was similarly modeled as second-order, irreversible, and catalyzed by phospho-MEK with a rate constant as described previously (Varga *et al.*, 2017). Both MEK and ERK dephosphorylation by protein phosphatases were modeled as zeroth-order with respect to protein phosphatases using the same nominal rate constant as with pRAF1 dephosphorylation.

***Sorafenib binding.*** The kinetics of sorafenib binding to RAF1 was approximated, assuming diffusional limitations. The diffusivity of sorafenib was set to the diffusivity of ATP, $2.5 \times 10^2$ $\mu m^2 \cdot s^{-1}$ (Hubley *et al.*, 1995), and the interaction radius of sorafenib with RAF1 was set to 1 nm. The rate constant for dissociation of sorafenib from RAF1 was calculated using its affinity for RAF1, which was estimated using sorafenib's $IC_{50}$ value for RAF1, the $K_m$ of RAF1 for ATP (Force *et al.*, 1994), and the Cheng–Prusoff equation (Cheng and Prusoff, 1973; Wilhelm *et al.*, 2004). Because sorafenib is a type II RAF inhibitor, it may only bind to RAF1 in its cytosolic, inactive state (Liu and Gray, 2006). BRAF's ability to activate RAF1 is dependent on its dimerization potential with RAF1 (Rajakulendran *et al.*, 2009; Roring *et al.*, 2012; Hu *et al.*, 2013). The constitutive phosphorylation of BRAF on S445 enables it to transactivate RAF1 through dimerization even when kinase-dead or inhibited by drugs such as sorafenib (Mason *et al.*, 1999; Heidorn *et al.*, 2010; Hu *et al.*, 2013). The model thus allows both BRAF and iBRAF to dimerize with RAF1 and catalyze its phosphorylation.

***Sensitivity analysis.*** Model sensitivity to univariate parameter changes was computed by individually increasing and decreasing parameter values by a factor of 10. Sensitivity was measured by summing the integrated differences between the original model and the two perturbed outputs over time. To compare differences among parameter perturbations, sensitivities were reported as percentages of the maximum predicted change to model output. For multivariate parameter sensitivity analysis, partial least-squares regression of random parameter sets, in which each parameter was randomly varied by up to an order of magnitude from its base value, was performed using *plsregress* in MATLAB.

## ACKNOWLEDGMENTS

We thank L. Loew and his team (University of Connecticut) for their help in Virtual Cell training, and K. Brown (Oregon State University) for assistance with modeling. These studies were supported by National Science Foundation Grant MCB 1715132 to M.J.L. and A.S.

## REFERENCES

Anderson DJ, Durieux JK, Song K, Alvarado R, Jackson PK, Hatzivassiliou G, Ludlam MJ (2011). Live-cell microscopy reveals small molecule inhibitor effects on MAPK pathway dynamics. PLoS One 6, e22607.

Blinov ML, Schaff JC, Vasilescu D, Moraru II, Bloom JE, Loew LM (2017). Compartmental and spatial rule-based modeling with Virtual Cell. Biophys J 113, 1365–1372.

Bondeva T, Balla A, Varnai P, Balla T (2002). Structural determinants of Ras–Raf interaction analyzed in live cells. Mol Biol Cell 13, 2323–2333.

Cargnello M, Roux PP (2011). Activation and function of the MAPKs and their substrates, the MAPK-activated protein kinases. Microbiol Mol Biol Rev 75, 50–83.

Chen WW, Schoeberl B, Jasper PJ, Niepel M, Nielsen UB, Lauffenburger DA, Sorger PK (2009). Input–output behavior of ErbB signaling pathways as revealed by a mass action model trained against dynamic data. Mol Syst Biol 5, 239.

Cheng Y, Prusoff WH (1973). Relationship between the inhibition constant (K1) and the concentration of inhibitor which causes 50 per cent inhibition (I50) of an enzymatic reaction. Biochem Pharmacol 22, 3099–3108.

Fischer A, Hekman M, Kuhlmann J, Rubio I, Wiese S, Rapp UR (2007). B- and C-RAF display essential differences in their binding to Ras: the isotype-specific N terminus of B-RAF facilitates Ras binding. J Biol Chem 282, 26503–26516.

Force T, Bonventre JV, Heidecker G, Rapp U, Avruch J, Kyriakis JM (1994). Enzymatic characteristics of the c-Raf-1 protein kinase. Proc Natl Acad Sci USA 91, 1270–1274.

Fortian A, Sorkin A (2014). Live-cell fluorescence imaging reveals high stoichiometry of Grb2 binding to the EGF receptor sustained during endocytosis. J Cell Sci 127, 432–444.

Freeman AK, Ritt DA, Morrison DK (2013). Effects of Raf dimerization and its inhibition on normal and disease-associated Raf signaling. Mol Cell 49, 751–758.

Fujioka A, Terai K, Itoh RE, Aoki K, Nakamura T, Kuroda S, Nishida E, Matsuda M (2006). Dynamics of the Ras/ERK MAPK cascade as monitored by fluorescent probes. J Biol Chem 281, 8917–8926.

Furcht CM, Buonato JM, Lazzara MJ (2015). EGFR-activated Src family kinases maintain GAB1–SHP2 complexes distal from EGFR. Sci Signal 8, ra46.

Galperin E, Sorkin A (2008). Endosomal targeting of MEK2 requires RAF, MEK kinase activity and clathrin-dependent endocytosis. Traffic 9, 1776–1790.

Hatzivassiliou G, Song K, Yen I, Brandhuber BJ, Anderson DJ, Alvarado R, Ludlam MJ, Stokoe D, Gloor SL, Vigers G, *et al.* (2010). RAF inhibitors prime wild-type RAF to activate the MAPK pathway and enhance growth. Nature 464, 431–435.

Heidorn SJ, Milagre C, Whittaker S, Nourry A, Niculescu-Duvas I, Dhomen N, Hussain J, Reis-Filho JS, Springer CJ, Pritchard C, Marais R (2010). Kinase-dead BRAF and oncogenic RAS cooperate to drive tumor progression through CRAF. Cell 140, 209–221.

Hibino K, Shibata T, Yanagida T, Sako Y (2011). Activation kinetics of RAF protein in the ternary complex of RAF, RAS-GTP, and kinase on the plasma membrane of living cells: single-molecule imaging analysis. J Biol Chem 286, 36460–36468.

Howe CL, Valletta JS, Rusnak AS, Mobley WC (2001). NGF signaling from clathrin-coated vesicles: evidence that signaling endosomes serve as a platform for the Ras-MAPK pathway. Neuron 32, 801–814.

Hu J, Stites EC, Yu H, Germino EA, Meharena HS, Stork PJS, Kornev AP, Taylor SS, Shaw AS (2013). Allosteric activation of functionally asymmetric RAF kinase dimers. Cell 154, 1036–1046.

Huang F, Sorkin A (2005). Growth factor receptor binding protein 2-mediated recruitment of the RING domain of Cbl to the epidermal growth factor receptor is essential and sufficient to support receptor endocytosis. Mol Biol Cell 16, 1268–1281.

Hubley MJ, Rosanske RC, Moerland TS (1995). Diffusion coefficients of ATP and creatine phosphate in isolated muscle: pulsed gradient 31P NMR of small biological samples. NMR Biomed 8, 72–78.

Jiang X, Sorkin A (2002). Coordinated trafficking of Grb2 and Ras during EGF receptor endocytosis visualized in living cells. Mol Biol Cell 13, 1522–1535.

Jin T, Lavoie H, Sahmi M, David M, Hilt C, Hammell A, Therrien M (2017). RAF inhibitors promote RAS–RAF interaction by allosterically disrupting RAF autoinhibition. Nat Commun 8, 1211.

Johannessen LE, Ringerike T, Molnes J, Madshus IH (2000). Epidermal growth factor receptor efficiently activates mitogen-activated protein kinase in HeLa cells and Hep2 cells conditionally defective in clathrin-dependent endocytosis. Exp Cell Res 260, 136–145.

Kholodenko BN (2002). MAP kinase cascade signaling and endocytic trafficking: a marriage of convenience? Trends Cell Biol 12, 173–177.

Kulak NA, Pichler G, Paron I, Nagaraj N, Mann M (2014). Minimal, encapsulated proteomic-sample processing applied to copy-number estimation in eukaryotic cells. Nat Methods 11, 319–324.

Lake D, Correa SA, Muller J (2016). Negative feedback regulation of the ERK1/2 MAPK pathway. Cell Mol Life Sci 73, 4397–4413.

Lauffenburger DA, Linderman JJ (1996). Receptors: Models for Binding, Trafficking, and Signaling, New York: Oxford University Press.

Lavoie H, Therrien M (2015). Regulation of RAF protein kinases in ERK signalling. Nat Rev Mol Cell Biol 16, 281–298.

Lavoie H, Thevakumaran N, Gavory G, Li JJ, Padeganeh A, Guiral S, Duchaine J, Mao DY, Bouvier M, Sicheri F, Therrien M (2013). Inhibitors that stabilize a closed RAF kinase domain conformation induce dimerization. Nat Chem Biol 9, 428–436.
Leicht DT, Balan V, Kaplun A, Singh-Gupta V, Kaplun L, Dobson M, Tzivion G (2007). Raf kinases: function, regulation and role in human cancer. Biochim Biophys Acta 1773, 1196–1212.
Liu Y, Gray NS (2006). Rational design of inhibitors that bind to inactive kinase conformations. Nat Chem Biol 2, 358–364.
Lommerse PH, Snaar-Jagalska BE, Spaink HP, Schmidt T (2005). Single-molecule diffusion measurements of H-Ras at the plasma membrane of live cells reveal microdomain localization upon activation. J Cell Sci 118, 1799–1809.
Mason CS, Springer CJ, Cooper RG, Superti-Furga G, Marshall CJ, Marais R (1999). Serine and tyrosine phosphorylations cooperate in Raf-1, but not B-Raf activation. EMBO J 18, 2137–2148.
Matallanas D, Birtwistle M, Romano D, Zebisch A, Rauch J, von Kriegsheim A, Kolch W (2011). Raf family kinases: old dogs have learned new tricks. Genes Cancer 2, 232–260.
McKay J, Wang X, Ding J, Buss JE, Ambrosio L (2011). H-ras resides on clathrin-independent ARF6 vesicles that harbor little RAF-1, but not on clathrin-dependent endosomes. Biochim Biophys Acta 1813, 298–307.
Mikula M, Schreiber M, Husak Z, Kucerova L, Ruth J, Wieser R, Zatloukal K, Beug H, Wagner EF, Baccarini M (2001). Embryonic lethality and fetal liver apoptosis in mice lacking the c-raf-1 gene. EMBO J 20, 1952–1962.
Muratcioglu S, Chavan TS, Freed BC, Jang H, Khavrutskii L, Freed RN, Dyba MA, Stefanisko K, Tarasov SG, Gursoy A, *et al.* (2015). GTP-dependent K-Ras dimerization. Structure 23, 1325–1335.
Nagaraj N, Wisniewski JR, Geiger T, Cox J, Kircher M, Kelso J, Paabo S, Mann M (2011). Deep proteome and transcriptome mapping of a human cancer cell line. Mol Syst Biol 7, 548.
Omerovic J, Hammond DE, Clague MJ, Prior IA (2008). Ras isoform abundance and signalling in human cancer cell lines. Oncogene 27, 2754–2762.
Pinilla-Macua I, Watkins SC, Sorkin A (2016). Endocytosis separates EGF receptors from endogenous fluorescently labeled HRas and diminishes receptor signaling to MAP kinases in endosomes. Proc Natl Acad Sci USA 113, 2122–2127.
Pol A, Calvo M, Enrich C (1998). Isolated endosomes from quiescent rat liver contain the signal transduction machinery. Differential distribution of activated Raf-1 and Mek in the endocytic compartment. FEBS Lett 441, 34–38.
Poulikakos PI, Zhang C, Bollag G, Shokat KM, Rosen N (2010). RAF inhibitors transactivate RAF dimers and ERK signalling in cells with wild-type BRAF. Nature 464, 427–430.
Rajakulendran T, Sahmi M, Lefrancois M, Sicheri F, Therrien M (2009). A dimerization-dependent mechanism drives RAF catalytic activation. Nature 461, 542–545.
Ran FA, Hsu PD, Wright J, Agarwala V, Scott DA, Zhang F (2013). Genome engineering using the CRISPR-Cas9 system. Nat Protoc 8, 2281–2308.
Rizzo MA, Shome K, Watkins SC, Romero G (2000). The recruitment of Raf-1 to membranes is mediated by direct interaction with phosphatidic acid and is independent of association with Ras. J Biol Chem 275, 23911–23918.
Roring M, Herr R, Fiala GJ, Heilmann K, Braun S, Eisenhardt AE, Halbach S, Capper D, von Deimling A, Schamel WW, *et al.* (2012). Distinct requirement for an intact dimer interface in wild-type, V600E and kinase-dead B-Raf signalling. EMBO J 31, 2629–2647.
Roy S, McPherson RA, Apolloni A, Yan J, Lane A, Clyde-Smith J, Hancock JF (1998). 14-3-3 facilitates Ras-dependent Raf-1 activation in vitro and in vivo. Mol Cell Biol 18, 3947–3955.
Samatar AA, Poulikakos PI (2014). Targeting RAS-ERK signalling in cancer: promises and challenges. Nat Rev Drug Discov 13, 928–942.
Shi T, Niepel M, McDermott JE, Gao Y, Nicora CD, Chrisler WB, Markillie LM, Petyuk VA, Smith RD, Rodland KD, *et al.* (2016). Conservation of protein abundance patterns reveals the regulatory architecture of the EGFR-MAPK pathway. Sci Signal 9, rs6.
Sorkin A, McClure M, Huang F, Carter R (2000). Interaction of EGF receptor and grb2 in living cells visualized by fluorescence resonance energy transfer (FRET) microscopy. Curr Biol 10, 1395–1398.
Sorkin A, Von Zastrow M (2002). Signal transduction and endocytosis: close encounters of many kinds. Nat Rev Mol Cell Biol 3, 600–614.
Sousa LP, Lax I, Shen H, Ferguson SM, De Camilli P, Schlessinger J (2012). Suppression of EGFR endocytosis by dynamin depletion reveals that EGFR signaling occurs primarily at the plasma membrane. Proc Natl Acad Sci USA 109, 4419–4424.
Stokoe D, Macdonald SG, Cadwallader K, Symons M, Hancock JF (1994). Activation of Raf as a result of recruitment to the plasma membrane. Science 264, 1463–1467.
Teis D, Wunderlich W, Huber LA (2002). Localization of the MP1-MAPK scaffold complex to endosomes is mediated by p14 and required for signal transduction. Dev Cell 3, 803–814.
Varga A, Ehrenreiter K, Aschenbrenner B, Kocieniewski P, Kochanczyk M, Lipniacki T, Baccarini M (2017). RAF1/BRAF dimerization integrates the signal from RAS to ERK and ROKα. Sci Signal 10, aai8482.
Vieira AV, Lamaze C, Schmid SL (1996). Control of EGF receptor signaling by clathrin-mediated endocytosis. Science 274, 2086–2089.
Wilhelm SM, Carter C, Tang L, Wilkie D, McNabola A, Rong H, Chen C, Zhang X, Vincent P, McHugh M, *et al.* (2004). BAY 43-9006 exhibits broad spectrum oral antitumor activity and targets the RAF/MEK/ERK pathway and receptor tyrosine kinases involved in tumor progression and angiogenesis. Cancer Res 64, 7099–7109.
Wojnowskia LFS, Zimmera AM, Hahna H, Beckc TW, Larnerb AC, Zimmera A (1998). Craf-1 protein kinase is essential for mouse development. Mech Dev 141–149.
Wu C, Lai CF, Mobley WC (2001). Nerve growth factor activates persistent Rap1 signaling in endosomes. J Neurosci 21, 5406–5416.